JOURNAL OF GEOPHYSICAL RESEARCH, VOL. 100, NO. B10, PAGES 19,991–20,009, OCTOBER 10, 1995

# Diffusion transport model for pelagic sediments on the Mid-Atlantic Ridge

Neil C. Mitchell

Department of Geological Sciences, University of Durham, Durham, England

**Abstract.** The diffusion model is potentially useful for quantifying the effect of downslope gravity transport on sedimentation rate variations, which are commonly found between Deep Sea Drilling Project and Ocean Drilling Program sites. If appropriate, the model and stratigraphy could be used, for example, to constrain the amount and timing of fault block rotation. Deep Tow profiler records from the French-American Mid-Ocean Undersea Study area of the Mid-Atlantic Ridge are examined to determine whether they are consistent with a diffusion model. Sedimentary contacts with basement show that a variety of processes may be operating, some of which are inconsistent with the diffusion model. For example, there are moats around some contacts which are typical of scouring or nondeposition due to high current velocities. More than half of the contacts, however, show onlapping, which is qualitatively consistent with the diffusion model. Sediments generally fill low areas of the topography and have smooth surfaces, as expected from a diffusion model. Where the fluxes of sediment entering a basin are constant, the diffusion model predicts that the sediment surface should evolve to a parabola (the steady state solution). Some 20 curved surfaces in the profiler data were digitized and least squares parabolas fitted to them with rms errors of less than 1 m. The slopes of the model parabolas provide values for the ratio of sediment flux to diffusivity at the edges of the basins (steep surfaces are produced by low diffusivity or high fluxes). This ratio is combined with estimates of the fluxes to determine the apparent sediment diffusivity, $K_{app}$, for each basin. Flux is estimated by assuming the abyssal hill topography acts as a simple sediment trap, so that the lateral flux equals the width of a basin's pelagic catchment area times the area's mean sedimentation rate $S$. Using this method, median $K_{app}$ is 0.04-0.11 $m^2\ yr^{-1}$ (assuming $S$=10-30 m m.y.$^{-1}$). Variations in $K_{app}$ and the assumptions behind the diffusion model are discussed, and alternative causes of sediment surface tilts are considered, in particular differential compaction, which is modelled using a simple porosity-depth function.

## Introduction

Where ridges are far from land, the accumulating sediments are mostly carbonates, with minor amounts of clay, and sometimes hydrothermal deposits if near hydrothermal vents. The carbonates are formed from the tests of pelagic organisms, which fall to the seafloor on their death. How these sediments are redistributed and accumulate over ridges has not received much quantitative consideration, perhaps because sediments are difficult to resolve with shallow-towed instruments and so the database, which is mostly from deep-towed instrumentation and coring, is small. This lack of a quantitative understanding is unfortunate because sediments could potentially provide information on many mid-ocean ridge processes, which are otherwise obscured by the redistribution. For example, variations in the thickness of the sediment cover could be used to determine age distributions of volcanic materials. For tectonic studies, we need to understand the sediment transport in order to infer tectonic tilting from the dip of stratigraphy [*Atwater and Mudie*, 1973] because this could otherwise be an artefact of the transport process. Furthermore, it may be possible to model tectonic uplift from its effect on nearby basin stratigraphy, as has been attempted using diffusion models for foreland basins [*Flemings and Jordan*, 1989; *Sinclair et al.*, 1991]. In the mid-ocean ridge case, tectonic uplift and tilting could alter the pelagic catchment areas [*Van Andel and Komar*, 1969] and thus change the fluxes of sediment entering topographic depressions. The ridge environment is also potentially well-suited for studying the process of sediment transport itself because the abyssal hill topography provides a range of parameters, such as slopes, basin shapes, fluxes, and exposure to bottom currents, and because some of the parameters can be constrained relatively easily. For example, sediment is supplied at a relatively steady rate from the water column so fluxes should be easy to determine.

The diffusion model has been used successfully to describe the evolution of hillslope morphology caused by soil creep [*Carson and Kirkby*, 1972; *Culling*, 1960; *Kirkby*, 1971] and has recently been applied to simulate sediment accumulation over abyssal hills by *Webb and Jordan* [1993]. Its basic assumption is that the downslope flux of sediment is proportional to the local slope. At present, there is very little quantitative understanding of the processes involved in pelagic sediment transport over ridges, so this simple relationship between flux and local slope cannot be predicted. Furthermore, these small fluxes would be impossible to measure over a long enough time span to verify the relationship directly. This study instead proceeds by seeing whether the shapes of sediment surfaces are consistent with a diffusion model and then later considers appropriate mechanisms which may cause bulk transport according to the diffusion equation. (Note that this kind of approach does not necessarily prove the diffusion model but only that it is consistent with the observations.) Whether



Paper number 95JB01974.
0148-0227/95/95JB-01974$05.00

diffusion is appropriate or not may largely depend on the relative importance of current-driven and gravity-driven transport. Of the latter type, hillslope creep, slides, and constant-width channel flows have been suggested to cause downslope movement according to a diffusion equation [*Begin et al.*, 1981; *Kenyon and Turcotte*, 1985; *Mitchell*, 1976]. As described in the later discussion, downslope movement of sediment resuspended by bottom organisms and slumping [*Arrhenius*, 1963; *Luyendyk*, 1970; *Marks*, 1981] may also be consistent with a diffusion model. However, the effect of bottom currents clearly cannot be modelled by this kind of equation because the flux depends on the stress at the base of the fluid [e.g., *Forbes and Drapeau*, 1989] not bottom slope. The importance of bottom currents is indicated, for example, by moating around basement outcrops over the Reykjanes Ridge [*Ruddiman*, 1972], current deposits and ripples along fracture zones [*Kastens et al.*, 1986; *Shor et al.*, 1980; *Vogt and Johnson*, 1973], and erosion around fault scarps over the Galapagos Spreading Center [*Klitgord and Mudie*, 1974]. Of the gravity processes, turbidity flows create flat-lying deposits [*Van Andel and Komar*, 1969], which would require high diffusivities, and therefore even gravity-driven transport is likely to involve a range of diffusivities for the different processes. These details are not resolved by the present study, but there are indications that current transport over ridges may perhaps be important where the topography is relatively smooth (Galapagos Spreading Center or East Pacific Rise) or where the bathymetry provides a pathway for bottom currents, such as along fracture zones, while areas sheltered from currents, such as among abyssal hills, show primarily downslope gravity transport for which the diffusion model may be useful.

The data analysed in this study are profiler records from the French-American Mid-Ocean Undersea Study (FAMOUS) area of the Mid-Atlantic Ridge collected by the Scripps Deep Tow instrument package in 1973 [*Macdonald and Luyendyk*, 1977], which is presently the only extensive near-bottom survey of the flanks of the Mid-Atlantic Ridge. Samples in the area show that the sediment is predomantly a calcareous foraminiferal ooze [*Marks*, 1981]. The profiler records unfortunately have low signal-to-noise ratios so the basement is mostly not visible through the sediment layer and little stratigraphy can be seen. A sophisticated numerical approach, such as by modelling the evolution of the sediment surface, would therefore not be justified. Instead, I compare the shape of the sediment surface in small basins and on slopes to simple analytic expressions and also assess the shapes of sediment contacts with basement. The results suggest that the diffusion model is consistent with some of the observations but that the model diffusivity for these areas is probably variable and sediment transport is three-dimensional. An illustration of how the model could be applied in practice is given in Appendix 1.

## The Diffusion Model for Sediment Transport

The primary assumption of the diffusion model [*Culling*, 1960] is that the lateral flux of sediment $q$ (kilograms per meter per year) is proportional to the local slope. In one dimension $x$ (meters), this can be written

$$q = -\rho K \frac{\partial U}{\partial x}, \tag{1}$$

where $U$ is the sediment's topography (meters), $\rho$ is the sediment density (kilograms per cubic meter) and $K$ is the diffusivity (square meters per year). A change in the flux over some distance implies that material is deposited or eroded. Including the rate of supply of pelagics from the water column $S$ (meters per year), which is the mean sedimentation rate for the area, the rate of deposition can be expressed in terms of the lateral rate of change of flux using a continuity equation

$$\frac{\partial U}{\partial t} = -\frac{1}{\rho}\frac{\partial q}{\partial x} + S. \tag{2}$$

Differentiating (1) and substituting in (2) produces the modified diffusion equation [*Webb and Jordan*, 1993]

$$\frac{\partial U}{\partial t} = K\frac{\partial^2 U}{\partial x^2} + S. \tag{3}$$

The model describes the erosion of sediment peaks (areas of negative curvature and therefore negative $\partial U/\partial t$) by gravity-driven transport into basins (areas of positive curvature). The following analyses assume that $K$ and $S$ are locally constant. If the diffusion model is appropriate, the diffusivity $K$ is likely to vary between different sediment types (such as due to different cohesive properties) and between different transport processes.

To determine if sediment surfaces are consistent with a diffusion equation, a potentially useful criterion is the degree to which the sediment surfaces in basins are parabolic, since the steady state solution for a constant width basin filling with constant fluxes is a parabola. The validity of using a steady state solution therefore needs to be justified first, in particular that the system will evolve rapidly toward the steady state. A simple geometry is considered (Figure 1a) in which the initial topography of the basin is zero and the basin is filled by constant fluxes $Q_1$ and $-Q_2$ on either side ($Q$ is the sediment volume flux, which is equal to $q/\rho$ and has the units square meters per year). Real basins clearly do not have this simple rectangular geometry, but this allows us to use an analytical solution, which illustrates that the system is responsive and hence that other geometries are also likely to evolve quickly to produce parabolic surfaces. Furthermore, the assumed geometry compared to real V- or U-shaped basins results in an overestimate of the time taken for the surface to become parabolic (since the early evolution involves filling the corners of the basin), so this will provide upper bounds on this evolution time. The solution (Appendix 2) is

$$U(x,t) = \frac{Q_1 - Q_2 + WS}{W}t - \frac{Q_1}{K}x + \frac{Q_1 - Q_2}{2WK}x^2 + (2Q_1 + Q_2)\frac{W}{6K} + \frac{2W}{\pi^2 K}\sum_{n=1}^{\infty}\frac{Q_2(-1)^n - Q_1}{n^2}\cos\left(\frac{n\pi x}{W}\right)\exp\left(-\frac{Kn^2\pi^2 t}{W^2}\right). \tag{4}$$

$W$ is the basin width. Figure 1a shows (4) for a series of times $t$ and zero $S$. The origin of the $x$ axis is at the center of the basin, $Q_1$ is set to zero, and the solution is mirrored about $x = 0$ to provide a symmetrical basin. The definitions of the dimensionless time $\tau$ and distance $x'$ are given in Appendix 2. After a significant lapse of time ($t > W^2/K$), (4) converges on the steady state solution

$$U(x,t) = \frac{Q_1 - Q_2 + WS}{W}t - \frac{Q_1}{K}x + \frac{Q_1 - Q_2}{2WK}x^2 + (2Q_1 + Q_2)\frac{W}{6K}. \tag{5}$$

The time to reach a steady state ($W^2/K$) is ~$10^5$-$10^7$ years with basin widths of a few hundred metres and with the diffusivities of $10^{-1}$-$10^{-2}$ m$^2$ yr$^{-1}$ found in this study. Due to the dependence on $W^2$, the sediments in small basins are likely to be closer to steady state solution than those in large basins. To get a more accurate

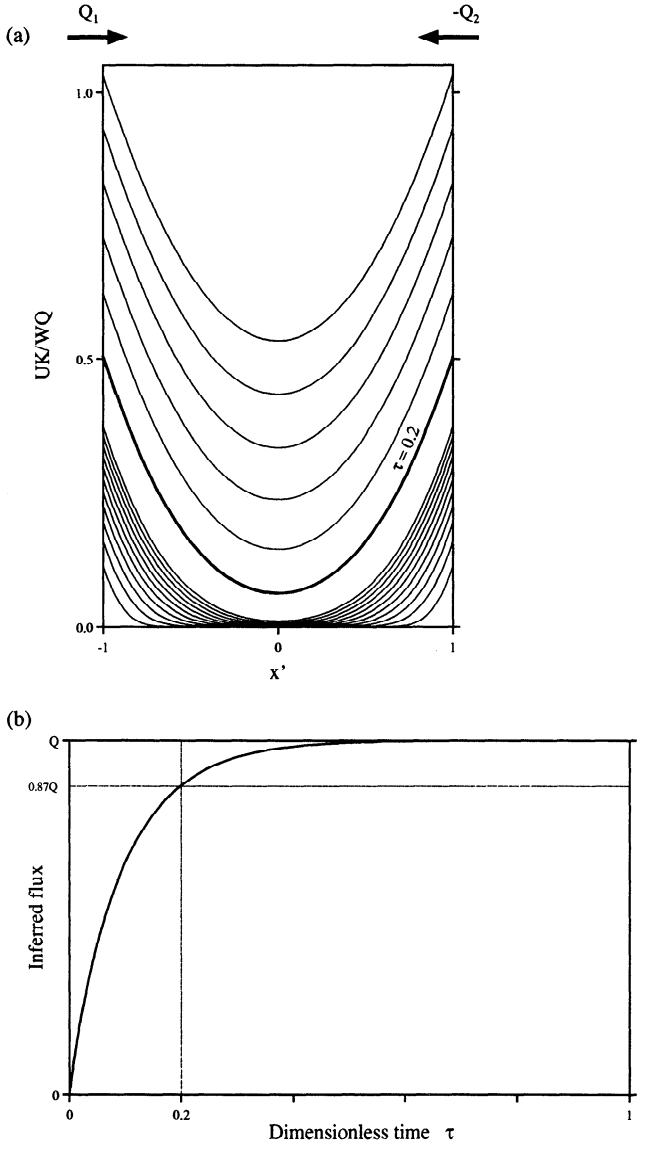


**Figure 1.** (a) A simple model of a flat-floored basin filling with constant fluxes $Q_1$ and $Q_2$ from either side. The curves show the evolution of the sediment topography in intervals of $\tau = 0.01$ up until $\tau = 0.1$ and in intervals of $\tau = 0.1$ thereafter, where $\tau$ is dimensionless time equal to $tK/W^2$. The curves were produced by evaluating (A2) with zero $S$ and $Q_1$ and negative $Q_2$ and then mirroring the solutions about $x' = 0$ to simulate a basin filling with equal fluxes from either side. The topography of the sediment is given as a dimensionless variable described in Appendix 2. (b) The evolution of the inferred flux, computed by fitting parabolas to the curves in Figure 1a and solving for $Q$ in (5), is shown. The inferred flux quickly approaches the actual flux $Q$ (e.g., $0.87Q$ at $\tau = 0.2$) showing that the system quickly evolves toward the steady state solution.

view of this convergence, a least squares parabola was fitted to each of the curves in Figure 1a and interpreted as if it were a steady state curve. The flux $Q_2$ was computed from the parabola coefficients using (5) and plotted against dimensionless time in Figure 1b. The inferred flux approximates the true flux much earlier than $\tau = 1$; for example, it is at 87% of its true value at $\tau = 0.2$. Therefore the edge slopes of parabolas fitted to profiler data will determine their fluxes relatively accurately if their ages are greater than ~$10^4$-$10^6$ years (as mentioned above, these are upper bounds on the evolution time). The seafloor covered by the Scripps Deep Tow extends to 75 km off-axis (~6 myr), so we might expect to find parabolic surfaces in small basins if the transport is governed by a diffusion equation.

To help further justify the use of a steady state solution, parabolas were fitted to the depositional centers in the results of *Webb and Jordan*'s [1993] numerical model. The regions around depositional centers in their Figure 1 are well-approximated by parabolas, and therefore we are justified in expecting to find parabolas in the profiler data if the transport is governed by a diffusion equation. Since their model incorporates fluxes evolving with time as successive minor basins in the upland topography are filled with sediment, the parabolic nature of their curves shows that deposition centers evolve rapidly toward the steady state solution in response to changes in fluxes. The system is therefore responsive to changes in the sediment supply, as also suggested by *Kenyon and Turcotte* [1985] for deposition along delta fronts.

## Examination of Deep Tow Records

Profiler records collected by *Macdonald and Luyendyk* [1977] from the two bold tracks in Figure 2 were examined. The data, shown in Figure 3a and 4a, were produced with a 4-kHz profiler [*Spiess and Lonsdale*, 1982] on a vehicle towed at altitudes of ~80-250 m (the mean altitudes are 120 m for line I and 189 m for line E"). Exposed bedrock was interpreted (Figures 3b and 4b) from zones of diffuse scattering in the records (extended dark areas), while thick sediment cover produces a shorter bottom echo without extended scattering. Sediments are shown by the stipple in Figures 3b and 4b. Note that, due to the low signal-to-noise ratio of these records, the basement is generally not visible through the sediment cover, and the extent of the stippling in these figures is not intended to show the depth of sediment.

### Initial Interpretation

The sediment accumulation appears to show two characteristics that are qualitatively consistent with a diffusive process. First, sediment is accumulating in the depressions and is generally absent in the upland areas, so there must be predominantly downgradient transport. Second, the sediment surfaces are smooth, which is also characteristic of a diffusive process.

The character of sediment contacts with basement reveals whether sediment transport is controlled by bottom currents or gravity processes. The contacts are classified (Figure 5) as "O", onlapping consistent with a diffusion model, "F", flat sediment at the contact, or "S", steeply dipping in an opposite sense to the basement. These are annotated on Figures 3b and 4b and summarised in Table 1. The flat sediment is consistent with a diffusion model but requires either very low sediment fluxes or very high diffusivities. The steeply dipping contacts could be produced by scouring or nondeposition due to strong bottom currents [e.g., *Ruddiman*, 1972] and are therefore inconsistent with a diffusion model. From the statistics in Table 1 the majority of the contacts are onlapping (O), although a significant number of contacts are nondiffusive (11%). These seem to occur in the centers of valleys, such as to the left of "9" (Figure 3b), rather than on the slopes, suggesting that bottom currents here are strongest in the flatter and deeper areas. This was suggested by readings from current meters deployed during the FAMOUS experiments [*Keller et al.*, 1975], which showed flow velocities within the rift valley that were an order of magnitude greater on average than those in the crestal mountains. Strong currents within the median valley

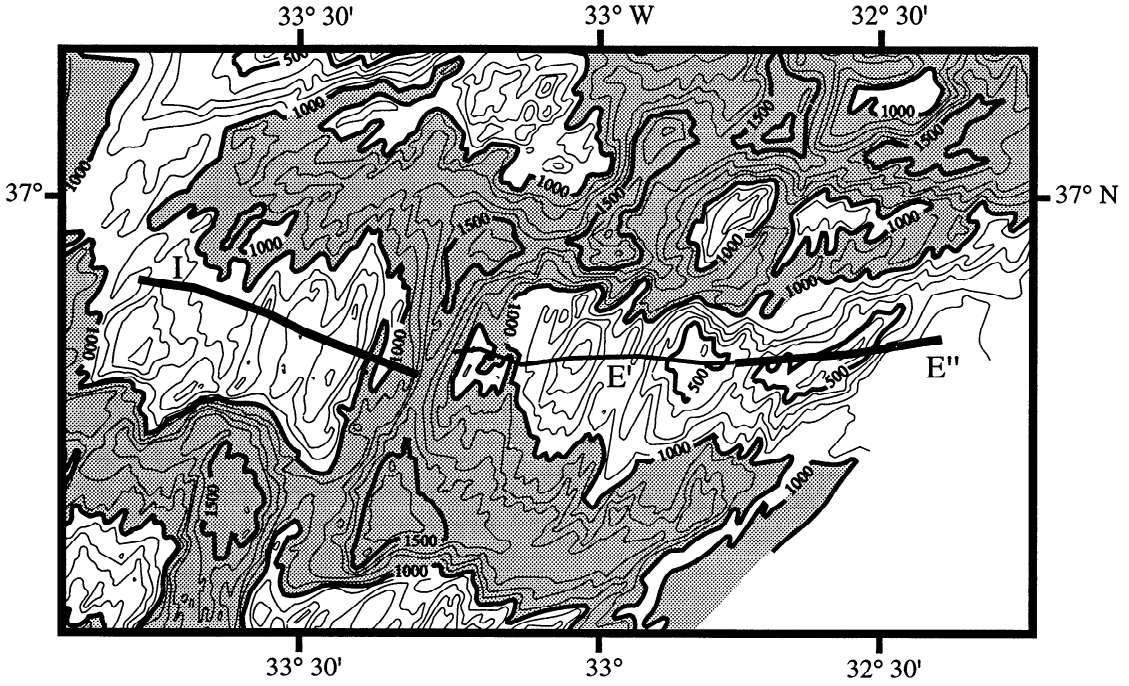


**Figure 2.** Location of Deep Tow survey lines in the Mid-Atlantic Ridge French-American Mid-Ocean Undersea Study (FAMOUS) area [*Macdonald and Luyendyk*, 1977], with multibeam bathymetry data redrawn from *Whitmarsh and Laughton* [1976]. Depths are in fathoms (1 fm = 1.8288 m) and bathymetry deeper than 1000 fm is shaded. Deep Tow data from the two highlighted lines are shown in Figures 3 (line I) and 4 (line E"). Line E' (thin line) lacked navigation in the data archive so it was only used to produce the statistics in Table 1.

floor are also suggested by suspended material in bottom photographs [*Ballard and Moore*, 1977], which suggest there is a well-developed bottom nepholoid layer.

The occurrences of flat sediment at basement contacts in Figures 3 and 4 may be consistent with a diffusion model but would require that the transport is three-dimensional and/or has variable diffusivity. For example, the sediment is onlapping at "9" as expected but is flat at the contact midway between "7" and "8" (also at the contact at ~34 km W). The width in the profiler records of the adjacent upland topography is similar in these cases, so there should be similar downslope fluxes of sediment if two-dimensional. We must conclude that, if the diffusion model is appropriate, the transport is three-dimensional or it involves processes with different diffusivities in different areas. Three-dimensional transport or variable $K$ would also be required to explain the presence of the flat contacts upslope of the diffusivelike contacts at "3" and "4". The occurrence of flat contacts is slightly higher for the lines further from the ridge crest (41% compared to 28%), which may suggest that mass flows with higher $K$ may be more common further from the axis.

## Sedimentation Rates

The assessment of diffusivity in the next section requires independent estimates of the rate of sediment supply from the water column so that fluxes can be estimated. However, the difficulty in assessing the sediment supply rate is that many of the published sedimentation rates are from individual cores without corrections for sediment redistribution. As acceptance criteria, these studies typically used the absence of any transport structures or whether the radiometric age varies linearly with depth in a core. However, if sediment is continually resuspended by biological or other activity on slopes (described later in the discussion), the reaccumulation of this suspended material at other sites could result in higher sedimentation rates at those sites without any transport structures and with linear age curves. Therefore it would be preferable to average sedimentation rates over areas that are larger than the length scale of the transport [*Mitchell*, 1993], such as by quantifying the mean rate of increase of sediment mass with basement age from the spreading center using sediment profiler records [*Mitchell*, 1995] (this is unfortunately not possible for the records in Figures 3 and 4 because of their low signal-to-noise ratios). A review of pertinent core data is given in Appendix 3 and suggests that the mean sedimentation rate is 10-30 m m.y.$^{-1}$ with the most probable rate near the bottom of this range.

## Steady State Solutions

The profiler data were examined for surfaces in the centers of small basins which are parabolas (steady state solutions). Coupled with estimates of the sediment fluxes into the basins, this permits an assessment of the diffusivity. The sediment topography for the numbered areas in Figures 3b and 4b was digitized and merged with the Deep Tow navigation to provide the topographic profiles in Figure 6. Some of these surfaces are from slopes or edges of basins, which may not necessarily be steady state solutions but are included so that the database is large enough to obtain a more precise estimate of diffusivity. Parabolas were fitted by least squares to the sections shown, and the slopes at each end of the model parabolas are given above the end of each profile (scaled by $10^3$). Two examples are shown in Figures 7 and 8. In Figure 7, the diffusion model interpretation involves sediment entering the basin with similar fluxes on either side. In Figure 8, the sediment appears to be perched in a basin between two small ridges. Interpreted with the diffusion model (Figure 8b), the sediment is entering the basin from above (pelagic fallout) and exiting mostly to the right, and the surface has evolved to a parabola typical of a steady state solution for a constant width

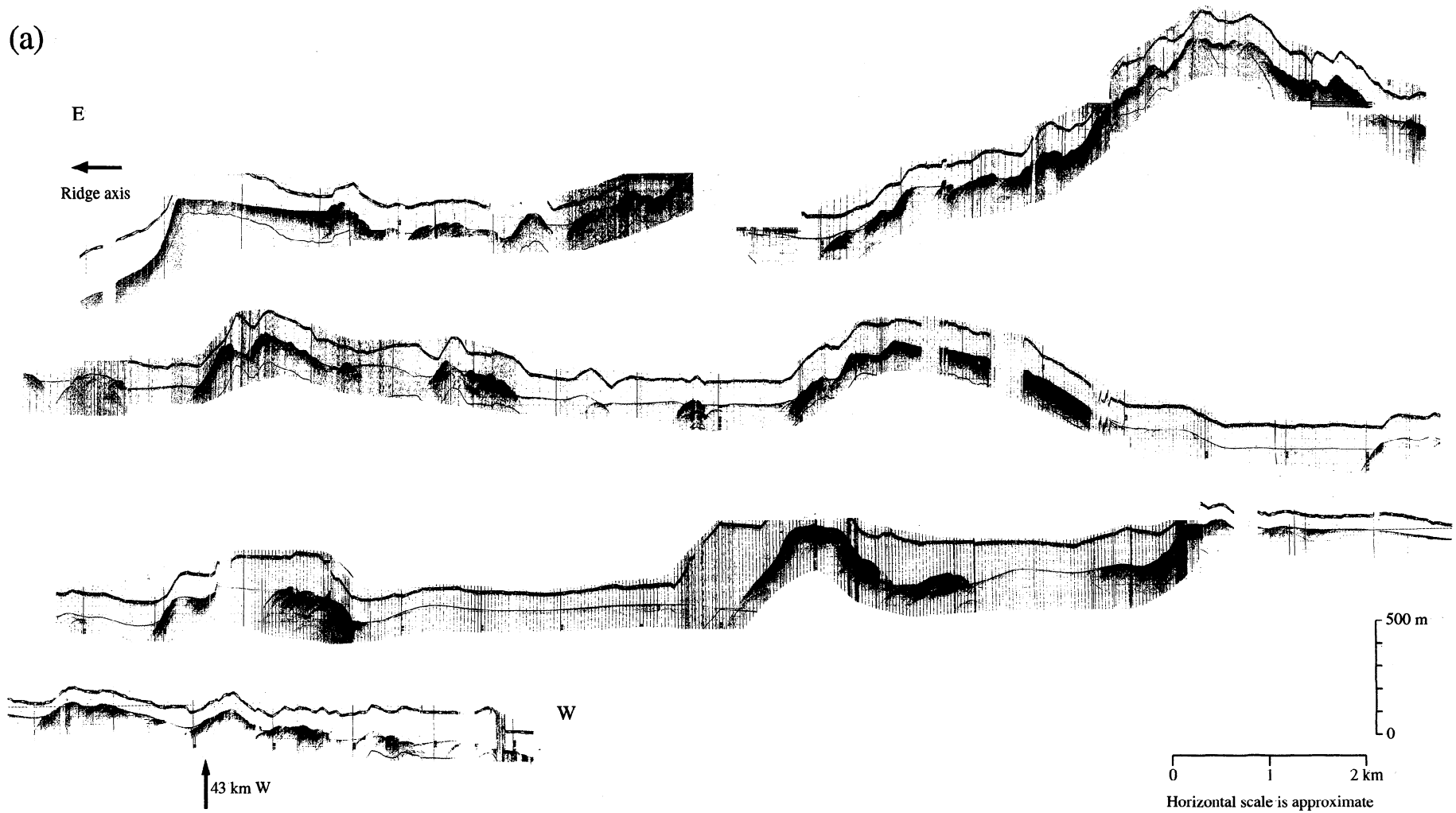


**Figure 3.** (a) Deep Tow profiler records from the west side of Figure 2 (line I). The bold dashed line running along the top of each record shows the path of the Deep Tow vehicle [*Spiess and Lonsdale*, 1982]. Sediments occur where the record has low energy (open areas) and a short bottom echo, while rock outcrops are the areas of diffuse scattering (solid areas and extended bottom echo). Note that the record is not corrected for gain changes, so some apparently high-energy areas may be sedimented, such as at 73 km in Figure 4a. The record is not adjusted for variations in fish speed, so the horizontal scale bar represent only the average scale. (b) Interpretation of the profiler records is shown. Stipple marks the locations of sediments (vertical extents are not intended to reflect the actual depth of sediments). The numbers above the profiles refer to the digitized sections in Figure 6. The sediment contacts with basement are classified as onlapping (O), horizontal sediment (F), or steeply dipping with opposite-sense slope (S).

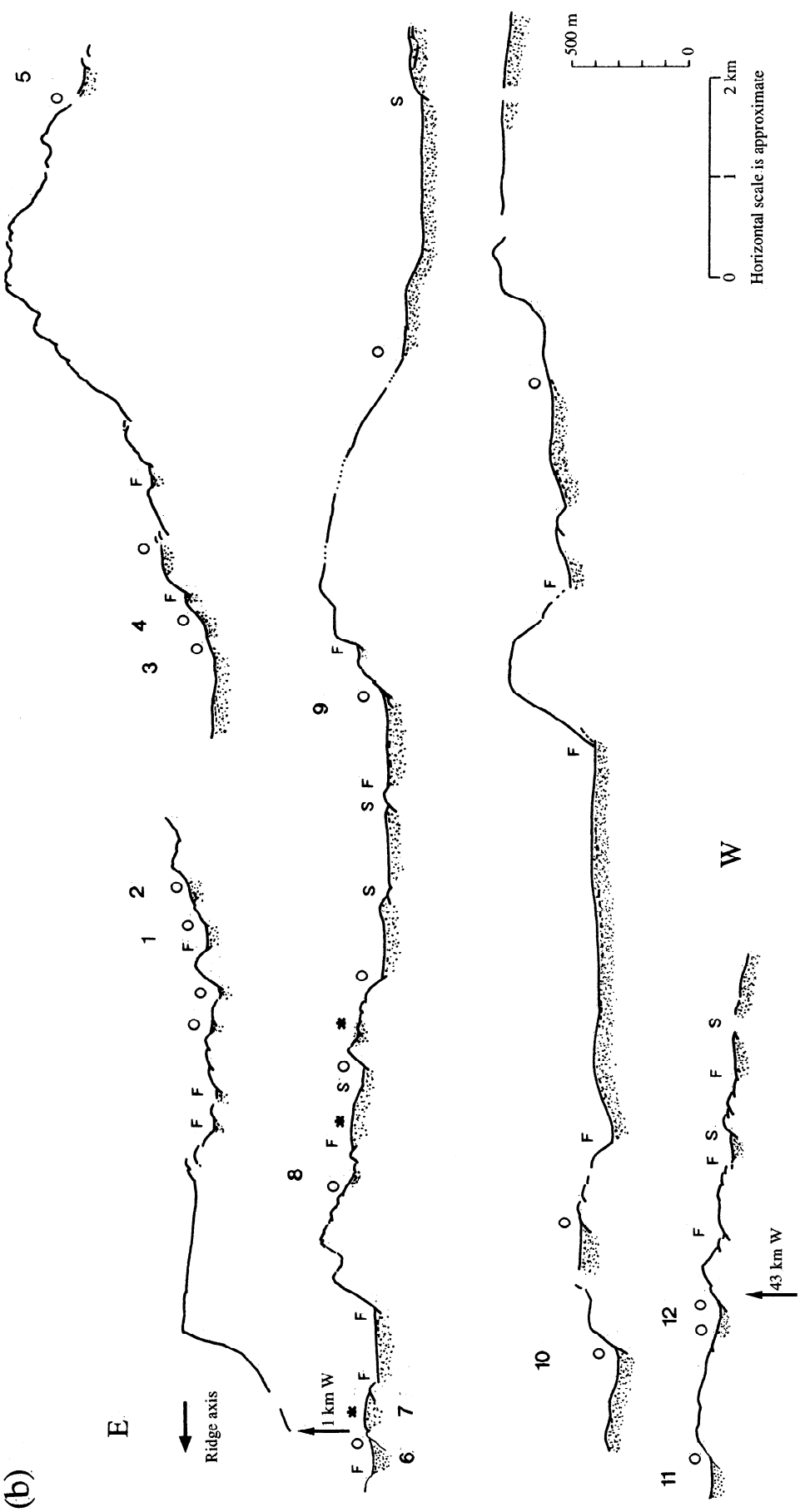


**Figure 3.** (continued)

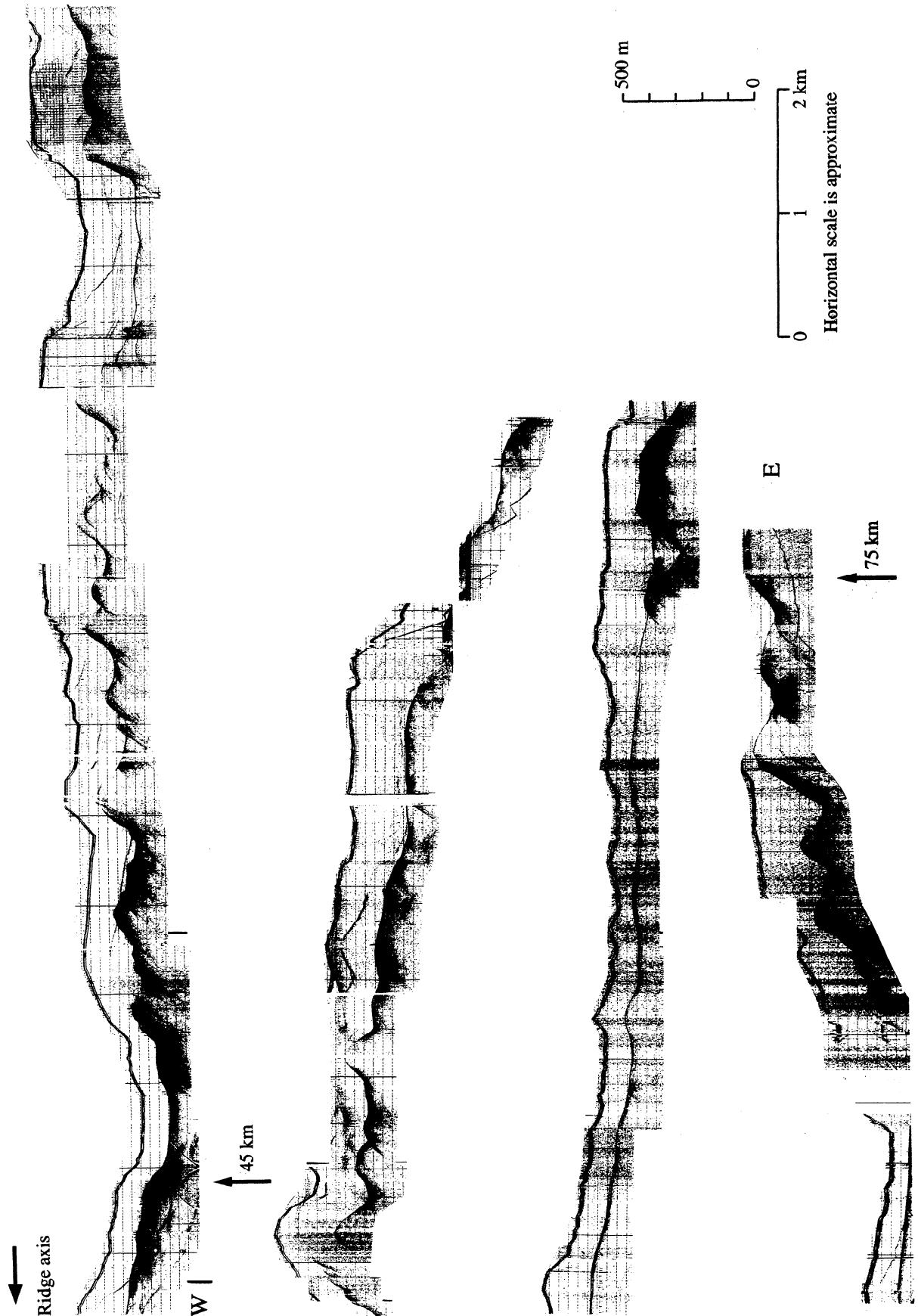


**Figure 4.** (a) Deep Tow profiler record from the east side of Figure 2 (line E"). (b) Interpretation of the profiler records is shown. Stipple marks the locations of sediments (vertical extents are not intended to reflect the actual depth of sediments). The numbers above the profiles refer to the digitized sections in Figure 6. The sediment contacts with basement are classified as onlapping (O), horizontal sediment (F), or steeply dipping with opposite-sense slope (S).

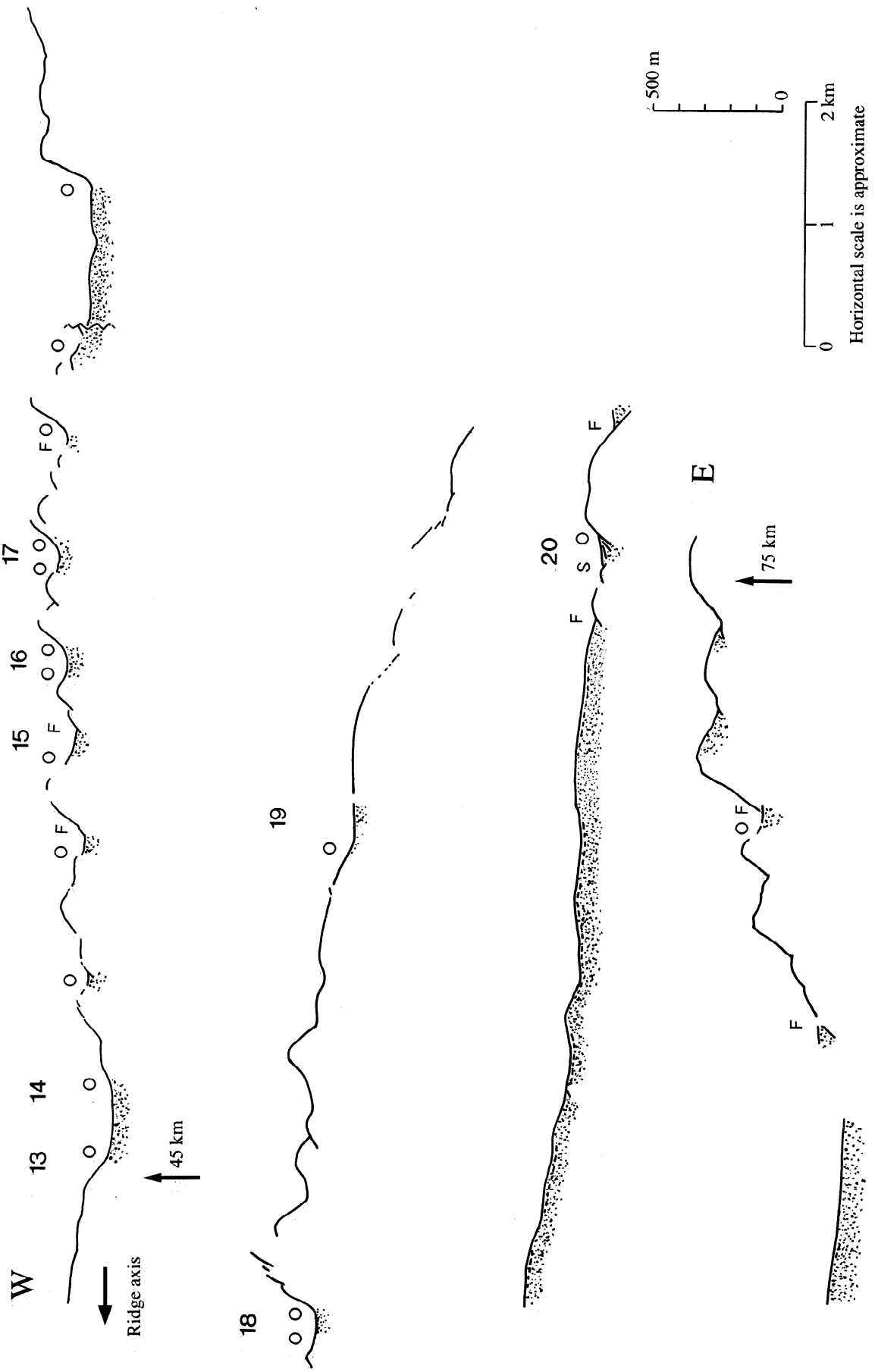


**Figure 4.** (continued)

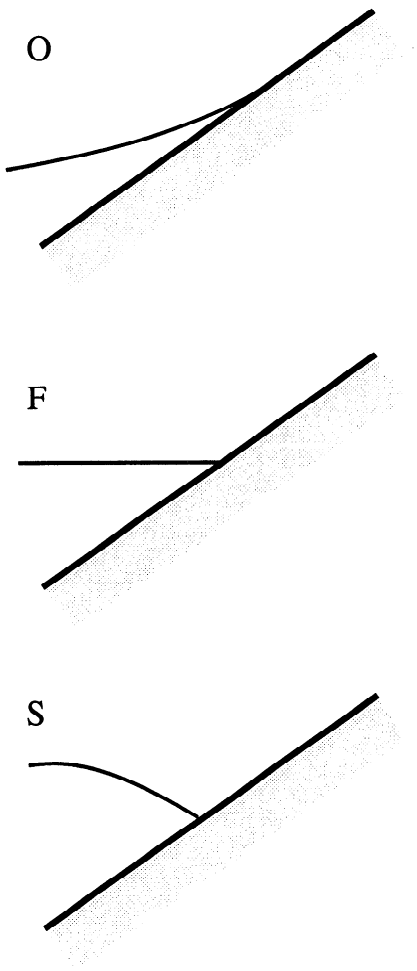


**Figure 5.** Definitions of the three types of sediment-basement contact: onlapping (O), flat sediment at the contact (F), or steeply dipping sediment with opposite sense of slope to the basement (S).

basin. Note that persistently steep surfaces, such as those in Figure 8, are not inconsistent with the diffusion model. In the model, steep surfaces are maintained by a balance between material supplied to the slope (local pelagic fallout and material supplied from upslope areas) and material removed by gravity-driven transport. This occurs when $Q_2 = Q_1 + WS$.

The geometry of Figure 8 allows us to determine the apparent diffusivity $K_{app}$ as follows. The flux of sediment into the basin is equal to the mean sedimentation rate $S$ for the FAMOUS area times the length of the profile to the right of the maximum ($L$ = 300 m). The sedimentation rate is not well constrained here, but we assume $S$ = 10-30 m m.y.$^{-1}$ (Appendix 3). Since the parabolic sediment surface suggests the basin is in a steady state, the outgoing flux should equal this incoming flux and $K$ can be calculated from the slope at the right of the profile, which equals $Q/K$. $K_{app}$ is therefore 0.017-0.050 m$^2$ yr$^{-1}$.

To make a more general assessment of diffusivity, $K_{app}$ was computed for each of the curves in Figure 6 by combining the value of $Q/K$ determined from the curve fitting with estimates of the fluxes into each basin. Fluxes were determined by assuming the ridges between basins are effective boundaries between accumulating provinces and sediment falling between a ridge and the edge of its adjacent basin is efficiently transported into the basin (Figure 9a). (This idea of pelagic "catchment areas" was proven at a coarser scale on slightly older seafloor by *Van Andel and Komar* [1969], who found a correlation coefficient of 0.83 between sediment volume in seismic records and catchment area.) The flux estimate is then given by $LS$, where $L$ is the catchment length. Catchment lengths interpreted from the profiler data (Figures 3 and 4) are shown by the thick horizontal bars in Figure 10. These choices are partly subjective, but they probably introduce an error in the results that is random rather than systematic.

The catchment lengths are plotted in Figure 9b with the corresponding model $Q/K$ obtained from the parabola fits (Figure 6). According to the model, $K_{app}$ equals the slope of each point to the origin (which equals $L/(Q/K)$) times $S$. The large scatter in the graph exceeds one order of magnitude and suggests a large range of $K_{app}$. However, whether this reflects the range of true diffusivity is unclear because the measurement of catchment length is error-prone and because the transport is probably three-dimensional, as suggested by the configuration of basement contacts mentioned above. An assessment of the range of $K$ will require three-dimensional surveys with profilers capable of resolving the stratigraphy, although these profiler data suggest that $K$ is not constant because profiles can have similar slopes ($Q/K$) and yet have very different catchment lengths. This is shown by profiles 15, 16, and 17, which have small catchment lengths, while 19 has a relatively large catchment length. The median diffusivity obtained from these data is 0.04-0.11 m$^2$ yr$^{-1}$ (the range of values is due to the range of the sedimentation rate estimates (Appendix 3)).

## Alternative Causes of Sediment Surface Tilt and Curvature

### Tectonic Tilting

Flat-lying sediment surfaces can be tilted by movement on normal faults. *Atwater and Mudie* [1973, 1968], for example, found turbidite beds deposited within the median valley of the Gorda ridge that have subsequently been tilted by ~6° (these are ~8 km from the rift axis, so they imply fast tilting rates of ~10° m.y.$^{-1}$). There is no discernable difference between sediment slopes dipping toward and away from the spreading axis in the FAMOUS data, so tectonic tilting is probably not important. The majority of these data are outside the region where tectonic tilting occurs [*Shaw and Lin*, 1993] so the lack of a preferred direction of dip suggests that surfaces have adjusted by sediment transport. It would be interesting to study sediments depositing at the same time as the tilting to see if gravity transport of material from uplifted blocks can create unconformities, which are predicted by the diffusion model.

### Compaction

Differences in compaction could potentially cause sediment surfaces to become tilted around basin edges. To determine if this effect is important, a simple model is developed for a basin filling

**Table 1.** Summary of Sediment Contacts With Basement

| | Line I | Line E' | I+E' | Line E" | Totals |
|---|---|---|---|---|---|
| Upward tapering | 17 (68%) | 10 (56%) | 27 (63%) | 19 (46%) | 46 (55%) |
| Flat | 7 (28%) | 5 (28%) | 12 (28%) | 17 (41%) | 29 (35%) |
| Steep dip opposing basement slope | 1 (4%) | 3 (17%) | 4 (9%) | 5 (12%) | 9 (11%) |
| Totals | 25 | 18 | 43 | 41 | 84 |

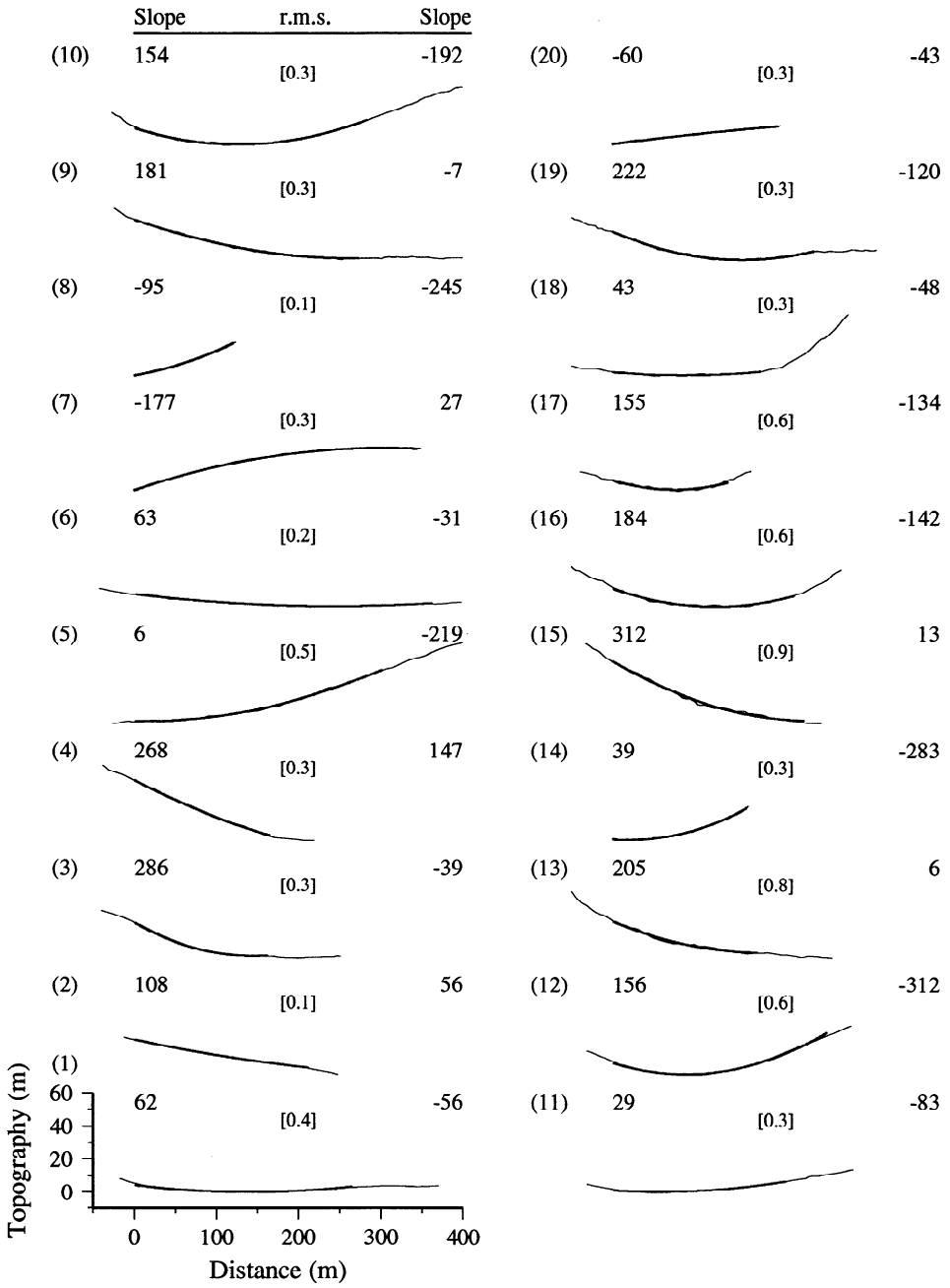


**Figure 6.** Least squares fits of parabolas (bold lines) to digitized sections of the profiler data (fine lines). The slope at each end of the parabola is given above each line, multiplied by a factor of 1000. According to the steady state diffusion model, these slopes equal the ratio $Q/K$ on either side of each basin. Since apparent slopes in the profiler data are slightly distorted (the profiler is omnidirectional), the slopes were effectively migrated by replacing them with tan(arcsin(apparent slope)). The precision of these slopes is proportional to the variability of towfish speed deduced from the tow fish navigation, which is probably less than 10%. The rms errors of the data about the parabolas are given in square brackets above each line (values in metres). These are less than 1 m and are probably comparable to the precision of these records when the variability due to the upward pointing fish-depth sounder is considered (these records were formed by adding the travel time of the fish-depth sounder to the profiler, so the variability in the sea surface detection probably has the greatest effect on depth precision [*Spiess and Tyce*, 1973]).

with compacting sediment but with no lateral transport. Two basement geometries are considered (Figure 11): a V-shaped basement with topography $y = mx$ (where $m$ is the basement slope and $x \geq 0$) and a U-shaped basin with topography $y = ax^2$ (a parabola shown by the dashed line in Figure 11 offset by 10 m). The basin is initially filled to a constant level and subsequently receives sediment uniformly with a constant sedimentation rate $S$. Simple mechanical compaction without dissolution is assumed [*Audet*, 1995] and is represented, for shallow sediments, by a linear porosity-depth function ($\phi = \phi_0 - \phi_b D$, where $D$ is depth, $\phi_0$ is the surface porosity, and $\phi_b$ is the rate at which porosity varies with depth). The dry mass of a sediment column of thickness $h$ is

$$M(x,t) = \int_0^h (1-\phi)\rho_g dD = \rho_g\left(\psi_0 h + \frac{\phi_b}{2}h^2\right), \qquad (6)$$

where $\rho_g$ is the average grain density of the sediment and $\psi_0$ is the

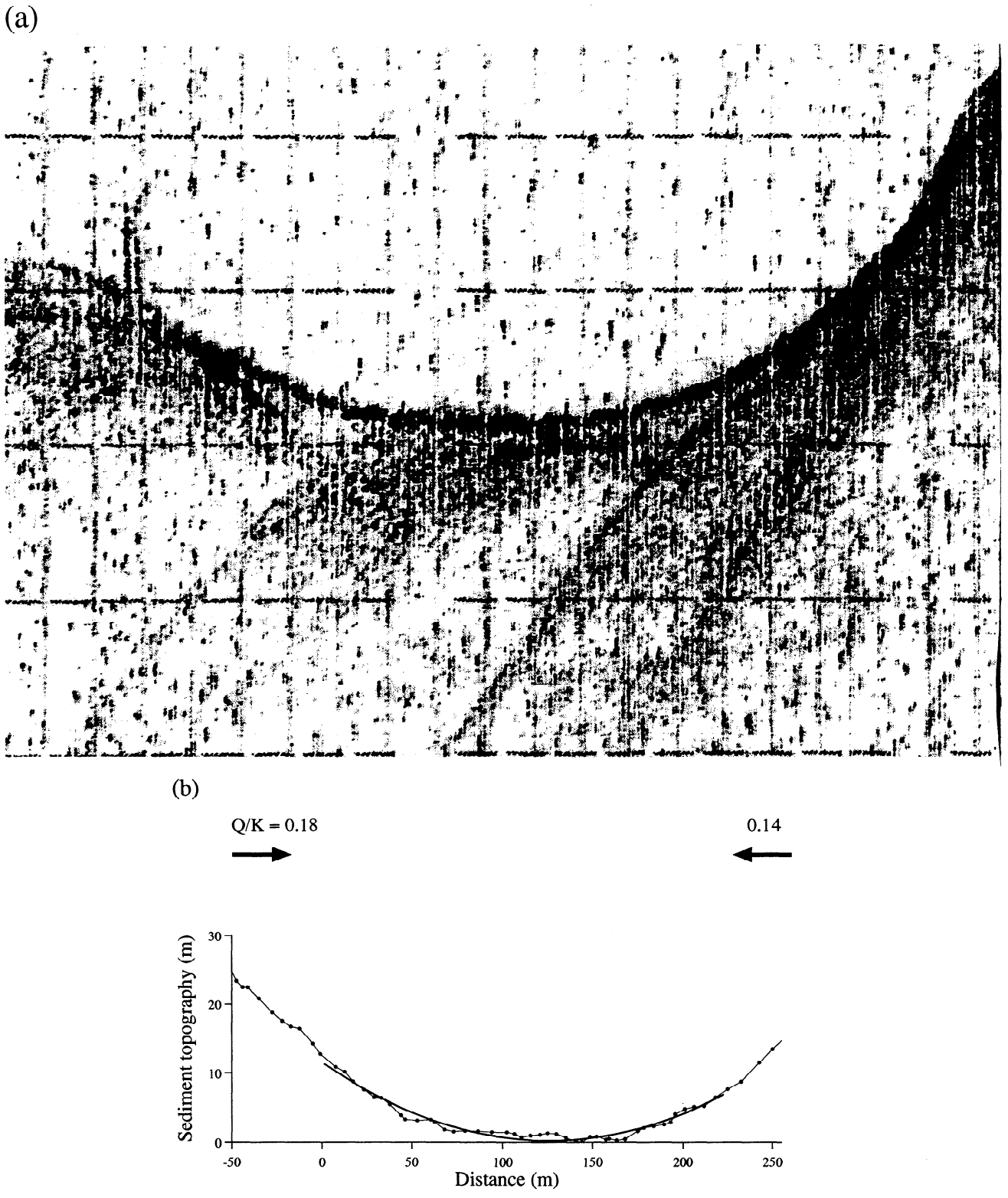


**Figure 7.** (a) An enlargement of the profiler data from curve 16 in Figure 6. (b) Diffusion model interpretation in which a basin is supplied by nearly equal sediment fluxes on both sides and the centre of the basin is parabolic.

solid fraction (1-$\phi_0$). The sediment accumulation rate is obtained by differentiating (6) with time $t$.

$$\frac{\partial M(x,t)}{\partial t} = \rho_g(\psi_0 + \phi_b h)\frac{\partial h}{\partial t} \tag{7}$$

The rate of mass increase also equals $S\psi_0\rho_g$. Equating this with (7) produces a first-order differential equation, which can be integrated to produce

$$S\psi_0 t = \psi_0(h-h_0)+\frac{\phi_b}{2}(h^2-h_0^2), \tag{8}$$

where $h_0$ is the initial thickness equal to $h_0(0)$-$mx$ (V-shaped basement) or $h_0(0)$-$ax^2$ (parabolic basement), where $h_0(0)$ is the initial sediment thickness at $x = 0$. Discarding the negative root, the solution to (8) is

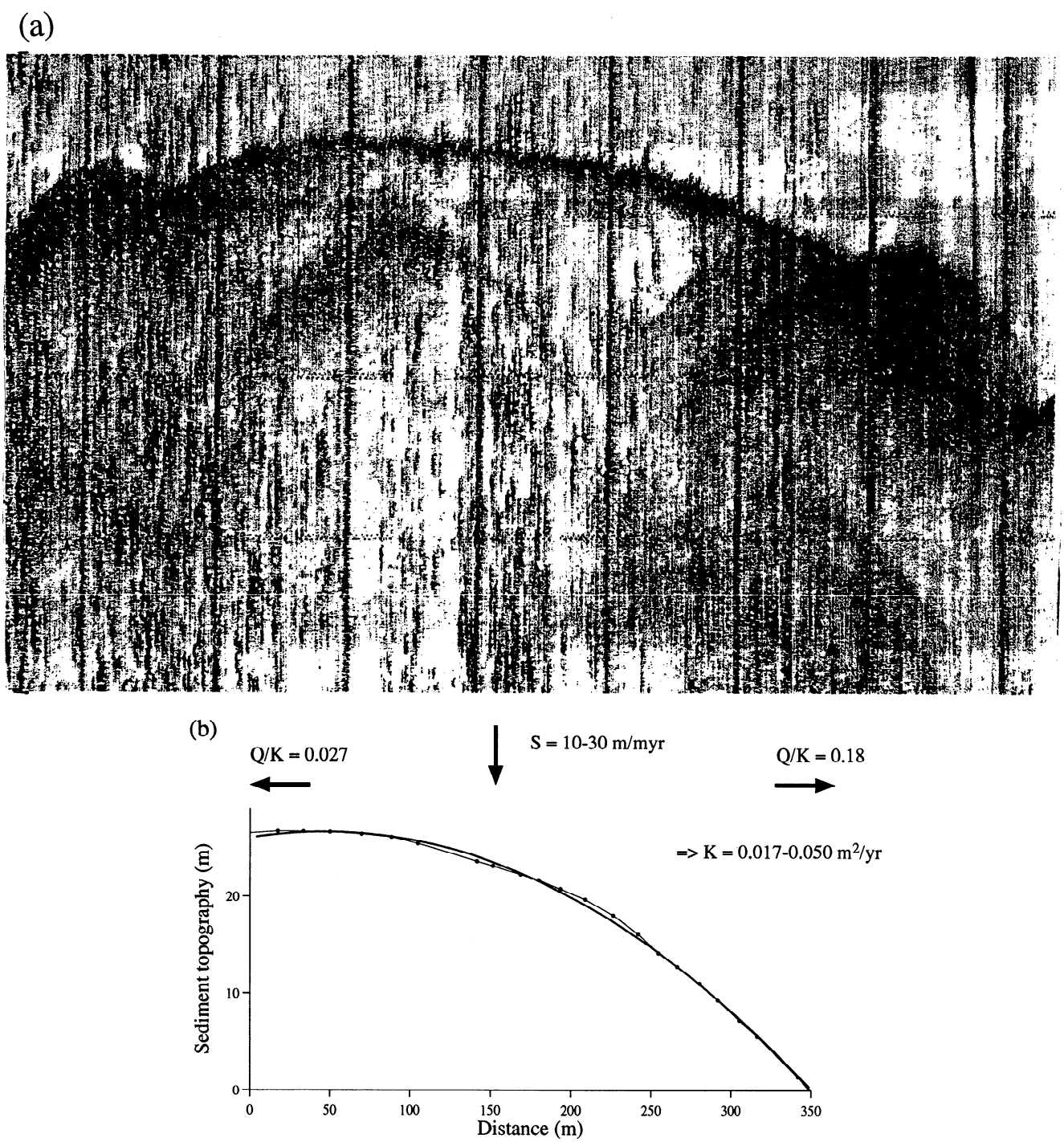


**Figure 8.** (a) An enlargement of the profiler data from curve 7 of Figure 6. (b) Diffusion model interpretation is shown. The profiler record shows sediment perched in a basin between two small hills. If interpreted with a diffusion model (Figure 8b), the basin is supplied by sediment from above (pelagic fallout), and material is exiting primarily to the right. The geometry allows the diffusivity $K$ to be determined as follows. The flux into the basin is the width of the basin to the right of the maximum (300 m) times the supply rate (10-30 m m.y.$^{-1}$). Assuming the system is in a steady state, the exit flux equals the entrance flux, and therefore $K$ can be computed from the slope on the right ($K$ = 0.017-0.050 m$^2$ yr$^{-1}$). Other surfaces which have a similar upward convex geometry are located by asterisks in Figure 3b.

$$h(x,t) = \left(\sqrt{\psi_0{}^2 + 2\phi_b c}\right) - \psi_0 \Big) / \phi_b, \quad (9)$$

where

$$c(x,t) = \psi_0(St + h_0) + \frac{\phi_b}{2} h_0^2.$$

The profiles of the sediment surface in Figure 11 were produced by computing $y = mx + h(x,t)$ for the V-shaped basement and $y = ax^2 + h(x,t)$ for the parabolic basement and using $h(x,t)$ from (9). $S$ was 10 m m.y.$^{-1}$, and $h_0(0)$ was 20 and 10 m (V-shaped and parabolic basins, respectively). The first two coefficients of a global porosity-depth regression of *Hamilton* [1976] were used: $\phi_0$ = 0.72 and $\phi_b$ = 0.000987 m$^{-1}$ (the second degree coefficient is insignificant over the depth interval of Figure 11). The surface

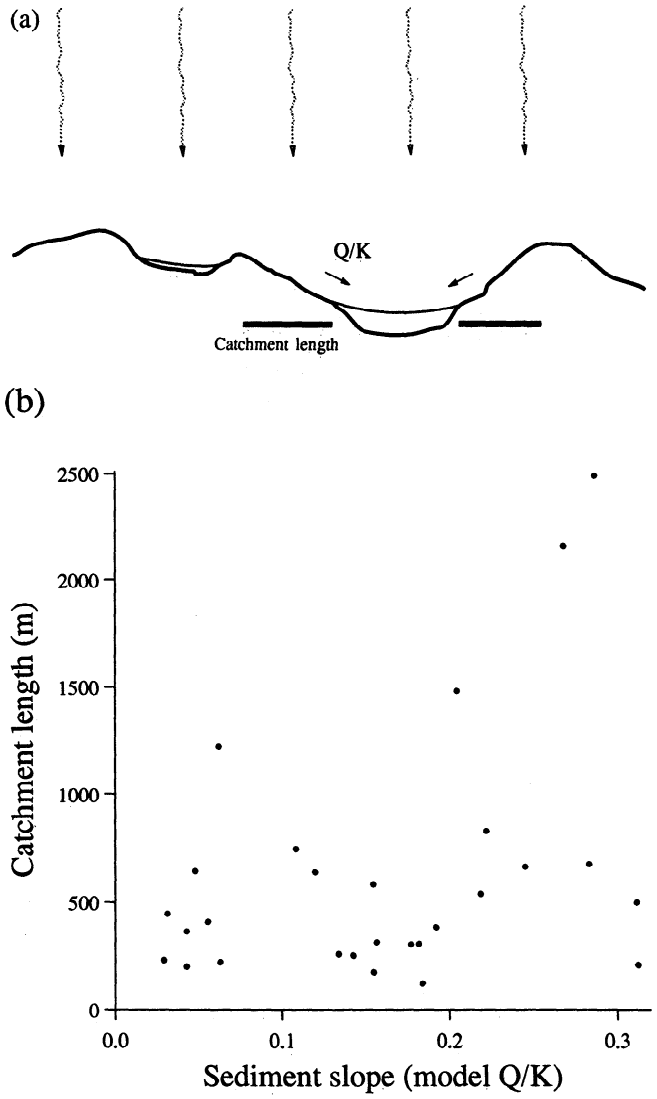


**Figure 9.** (a) Sediment fluxes were estimated by assuming ridges are boundaries between accumulating provinces, so that the fluxes are equal to the mean sedimentation rate times the "catchment lengths" interpreted from the bathymetry. These lengths were measured from the ridges to the edges of the parabolas in Figure 6 and are shown in Figure 10. (b) Graph of the sediment catchment length ($L$) against the slope at the edge of the basins (equal to $Q/K$ in the diffusion model) is shown. The apparent diffusivity $K_{app}$ for each basin equals the slope of each point to the origin times the mean sedimentation rate. The large scatter of slopes in the graph, which is more than one order of magnitude, represents a large range of $K_{app}$. However, the true range of $K$ is probably less than this because errors in the estimate of $L$ and three-dimensional transport add variability.

porosity (0.72) is compatible with sediment densities for the Mid-Atlantic Ridge used by *Balsam* [1988].

The results of the model (Figure 11) show that differential compaction does not greatly deflect the sediment surface; the maximum slope after filling the basin with more than 60 m of sediment is only 0.028. This is shallower than the majority of the surface slopes in Figure 6, which must therefore be due to other processes, such as sedimentary transport. The rate at which compaction tilts the surface in Figure 11 is slow (average 0.005 per m.y.) and depends on the depth and slope of the basement. This can be demonstrated by calculating the rate of change of surface slope with time for the V-shaped basin, which is simply

$$\left.\frac{\partial^2 y}{\partial t \partial x}\right|_{\substack{x=0 \\ t=0}} = \frac{S\phi_b \psi_0 m}{(\psi_0 + \phi_b h_0(0))^2}. \quad (10)$$

The rate at which the surface slope varies is therefore proportional to the basement slope $m$, and the sensitivity to basement topography decreases with basement depth. The sensitivity becomes small when $h_0 > (1-\phi_0)/\phi_b$, which should generally occur when $h_0 > 280$ m for carbonate oozes from the data in *Hamilton* [1976]. The transition will be shallow if the porosity or porosity gradient are high. For example, characteristics of sediments from the Galapagos Spreading Center (Deep Sea Drilling Project (DSDP) site 508, $\phi_0 = 0.848$ and $\phi_b = 0.0025$ m$^{-1}$ [*Karato and Becker*, 1983]) suggest that this will occur at only 61 m. (A simple linear porosity-depth function has been assumed in this argument, so the actual effect of basement depth should be greater than predicted by (10), and these transition depths may be shallower.) Interestingly, (10) predicts that surfacial sediments over buried abyssal hills should generally be flat-lying in areas between hill crests (large $h_0$) but should be locally tilted and elevated immediately over the hill crests.

## Discussion

The median diffusivity determined here, 0.04-0.11 m$^2$ yr$^{-1}$, is comparable to the average diffusivity of 0.13 m$^2$ yr$^{-1}$ computed by *Webb and Jordan* [1993] from multibeam echosounder data at 26°-27° N on the western flank of the Mid-Atlantic Ridge. The difference in average diffusivity between the two studies is interesting, though it may be an artifact of the variability in these data (Figure 9b) or regional variations since the diffusivities calculated by *Webb and Jordan* [1993] varied from 0.04 to 0.26 m$^2$ yr$^{-1}$. Furthermore, *Webb and Jordan* [1993] included flat lying sediment ponds, which require high diffusivities if described using diffusion models, and this may have increased their average diffusivity. The relative similarity of the two sets of results, however, is surprising considering the different analytical approaches of the two studies. (*Webb and Jordan* [1993] have applied a numerical diffusion model generally to bathymetry data in their region, while this study involved selecting "ideal" examples.) The relatively good correspondence suggests that the diffusion model is more generally applicable (although this will require further verification).

Three mechanisms are considered here which might produce bulk sediment transport with a flux proportional to slope as required for the diffusion model. *Kenyon and Turcotte* [1985] suggested that the transport of delta front sediments occurs partly by small landslides and that the frequency of landslides is proportional to their driving force, which is approximately proportional to slope where the slope is small. A bulk flux proportional to slope was proposed to result when the effect of large numbers of slides is averaged over time. Part of the observed variability in $K_{app}$ could then be due to variations in pore pressure due to hydrothermal convection [*Langseth et al.*, 1992], which cause variations in the failure criterion [*Prior and Suhayda*, 1979], or could be related to proximity to active faults if seismic triggering is important. Kenyon and Turcotte also suggested that bioturbation may cause creep in delta front sediments; bioturbation within the upper 10 cm or so of pelagic sediments [e.g., *Berger and Heath*, 1968] may perhaps cause creep in a similar way to that proposed for hillslope soils [e.g., *Culling*, 1965]. The variability in $K_{app}$ could then be due to variations in the species of benthic fauna and their activity.

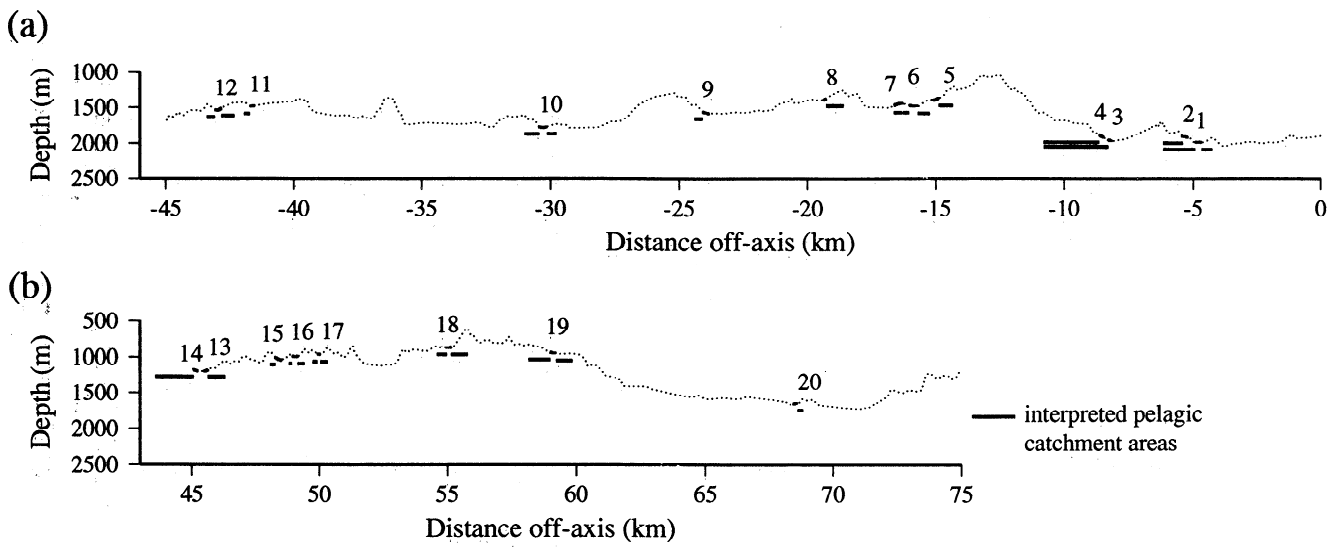


**Figure 10.** (a) Line I and (b) line E bathymetry annotated with the model curves and interpreted catchment lengths (thick horizontal bars). The interpretation of the pelagic divides partly compensates for the apparent three dimensionality of the transport. For example, the sediment entering "2" is assumed to bypass the small upslope ridge, whereas the ridge upslope from "5" and "6" is assumed to be an effective barrier because it contains flat sediment (which suggests that sediment is transporting perpendicular to the profile).

The third mechanism is due to sediment being repeatedly resuspended and moving downslope under gravity [*Arrhenius*, 1963; *Luyendyk*, 1970; *Marks*, 1981]. Resuspension could occur by sliding or slumping from oversteepened slopes or by expulsion by burrowing organisms or by fish swimming over the bottom, as shown by bottom photographs [*Arrhenius*, 1963; *Seibold and Futterer*, 1982]. Marks suggests that this is the most probable mechanism for moving material downslope because it is supported by visual observations made during the FAMOUS submersible dives and is consistent with a decrease in grain size with depth, which Marks observed, because finer sediments remain suspended for longer [*Berger and Piper*, 1972] during the downslope movement of each suspension. It is unclear whether this mechanism would exactly produce a simple relationship such as (1), i.e., with transport flux proportional to slope, because the suspension would be most likely turbulent, although we can at least state that the downslope component of the suspension's negative buoyancy (the lateral driving force) is approximately proportional to the local slope. The variation of grain size may partly explain the variability in $K_{app}$ because a suspension containing a larger proportion of fines will retain its load for longer and would therefore produce a higher diffusivity. *Kenyon and Turcotte* [1985] also noticed a variation in $K$ with grain size; $K$ for the Rhine and Frazer River deltas, which are mostly sand and silt, was an order of magnitude lower than that for the Mississippi delta, which has more than 70% clay. The variability of $K$ could also be due to variable frequency of slumping and sliding, as mentioned above, and to variable activity of the bottom fauna.

*Marks* [1981] grain size analyses are reproduced in Figure 12, which reveal a surprisingly linear relationship with water depth. The decreasing grain size suggests that the majority of the sediment transport occurs by repeated resuspension (developed below) rather than bulk transport, such as slumping or sliding. The graph can also be used to predict the general variation in sedimentation rates with depth if we make some simplifying assumptions: we assume that sediment density is invariant (i.e., we ignore differences in packing efficiency with grain size) and assume that the coarse fraction (>63 mm) is immobile so that the grain size variation reflects dilution or concentration of the coarse fraction due to transport of the fines. The variation of the coarse fraction with depth ($f_0+bZ$, where $f_0$ is the fraction at zero depth and $b$ is its variation with depth $Z$) can then be inverted for the sedimentation rate, which is $S_c/(f_0+bZ)$, where $S_c$ is the effective sedimentation rate of the coarse fraction. This relationship is shown by the dotted line in Figure 12 and is a hyperbola, showing that the majority of the sediment accumulation occurs in the deeper depressions, with relatively little on the slopes. Since the coarse fraction was assumed to be immobile, this provides a minimum bound on the sedimentation rate variation, which is probably more pronounced than shown in Figure 12. This also indirectly supports the assumption that lateral fluxes can be estimated from catchment areas because little sediment is retained on the slopes. Note that the grain size variation suggests that sediment transport in the median valley is not primarily due to bottom currents because this would lead to less deposition of fines, not more as is observed (stronger currents have been found to occur at depth in this area [*Keller et al.*, 1975]).

A useful test of the diffusion model would be to verify the computed diffusivity (0.04-0.11 $m^2\ yr^{-1}$) with independent knowledge of the transport process. This is not possible here because there are very few appropriate data available for the FAMOUS area. However, the rates of downslope movement predicted by the diffusion model can be shown to be reasonable in a general sense if it occurs by repeated resuspension. The following argument reproduces a flux of 0.005 $m^2\ yr^{-1}$, which corresponds to a slope of ~5° and diffusivity of 0.06 $m^2\ yr^{-1}$. The rate of occurrence of resuspension events could potentially be estimated from their occurrence in bottom photographs, but there are no events in the few published photographs taken of the FAMOUS area [*Ballard and Moore*, 1977; *Luyendyk and Macdonald*, 1977]. However, T. H. van Andel (personal communication, 1994) reports visual observations of many resuspensions during ALVIN dives, so we might assume that the occurrence is roughly one frame in 1000 (this and the following are only order-of-magnitude estimates). Each frame or visual

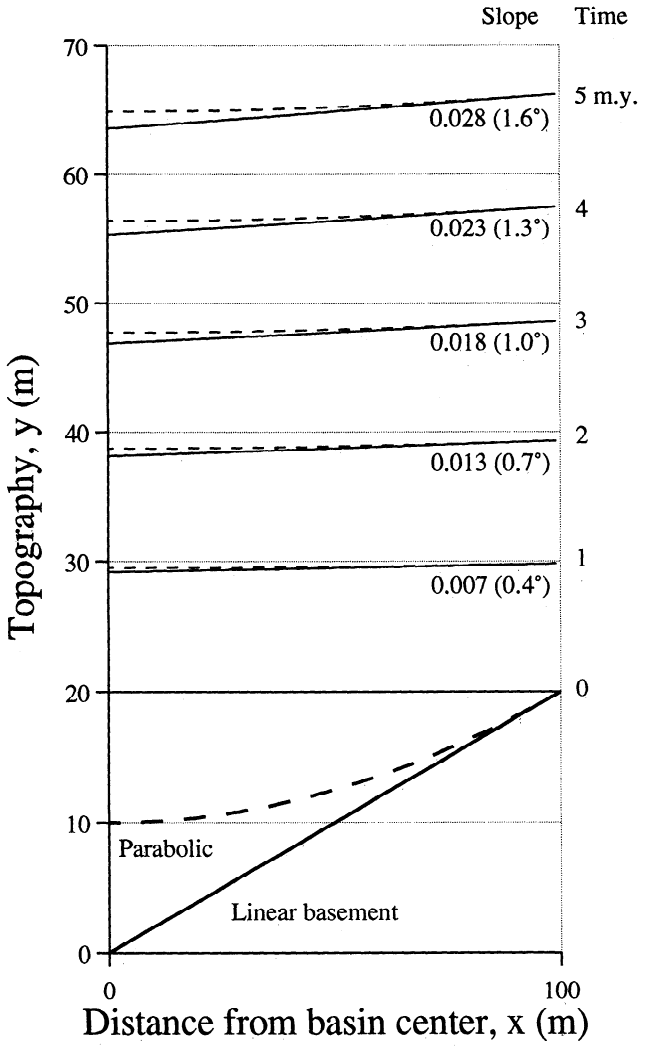


**Figure 11.** Model for the effect of differential compaction on sediment surfaces. A basin is initially filled with sediment to a constant level (20 m) and subsequently receives sediment at a uniform sedimentation rate with no lateral transport. A simple linear porosity-depth function was used to simulate compaction. Solutions are shown for basements that are V-shaped (continuous lines) and parabolic (dashed, offset 10 m). The sediment surface changes slope slowly so differential compaction is unlikely to have caused the sediment dips seen in the profiler records.

observation from ALVIN capable of resolving sediment suspensions covers an area about 5 m across. Assuming the sediment volume for each suspension event is ~10 $cm^3$ (judging from the sizes of suspensions and bottom scars in photographs) and that each event takes ~2 min to deposit and transports sediment 50 m downslope on average (i.e., a speed of ~1 knot), we obtain a volume flux of 0.005 $m^2\ yr^{-1}$. As mentioned above, this is not a fully quantitative estimate, but it hopefully illustrates that the rates predicted by the diffusion model are at least reasonable in a general intuitive sense.

These fluxes are relatively small when compared to fluxes that can potentially be produced by bottom currents. For example, data on suspended material and frequency of deep sea storms from the base of the Nova Scotian Rise [*Gross et al.*, 1988; *Gross and Nowell*, 1990] indicate annually averaged fluxes as high as $10^5$ kg $m^{-1}yr^{-1}$ (equivalent to $10^2\ m^2\ yr^{-1}$). Some of the suspended material was organic matter which would have dissolved during

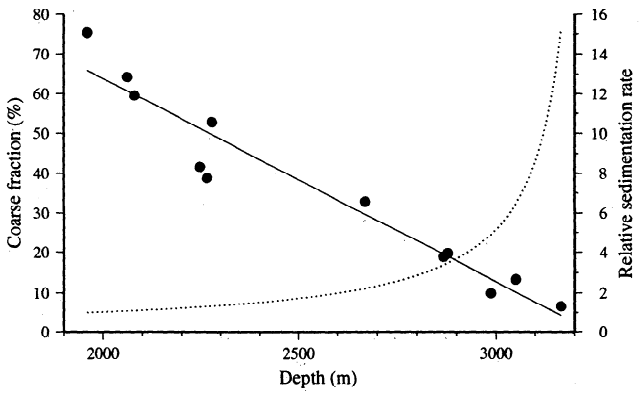


**Figure 12.** Variation of sediment grain size with depth for cores covering ~100 km of the FAMOUS area reported by *Marks* [1981]. Grain size is represented by the percentage of each core containing grains of greater than 63-μm diameter. The deeper cores contain a much higher proportion of fine grains and suggest that sediment is sorted by winnowing caused by resuspension. The dotted line and axis on the right show the variation in sedimentation rates with depth implied by the grain size variation. The rates were computed by assuming that the sediment density is constant and that the coarse grains are relatively immobile so that the variation in coarse fraction is due to concentration or dilution by the fines.

deposition so this is an overestimate of sediment flux, but it is nevertheless several orders of magnitude higher than the fluxes predicted by the diffusion model. Although such high fluxes might be uncommon, bottom currents capable of transporting sediment with similar fluxes to the diffusion model are probably common so it would be desirable to develop a model that includes both gravity transport and the effects of currents. This might be possible by developing the repeated suspension model described above, including an additional local current drift on the suspension as it deposits.

To answer whether gravity transport is linear or nonlinear will also need higher quality records than these Deep Tow data, although some tentative statements are possible. To represent nonlinear diffusion, (1) can be made equal to $-K(\partial U/\partial x)^n$, where $n$ is a real number and $\partial U/\partial x$ is positive. The steady state solution for a basin of width $W$ filling with a constant flux $-Q_0$ from the right side and zero flux from the left is

$$U(x,t) = U_0(t) + \frac{n}{1+n} x^{\frac{1+n}{n}} \left( \frac{Q_0}{KW} \right)^{1/n}. \qquad (11)$$

Basin shapes can be produced by mirroring this equation about $x = 0$. For $n<<1$, these solutions are U-shaped, while for $n>>1$ they are V-shaped. Better quality records are required because U-shaped surfaces (e.g., at "13" and "14" in Figure 4b) could also be due to the system being at an early stage of evolution, as illustrated in Figure 1a. However, the data in Figures 3 and 4 show no minima that are steeply V-shaped, so any nonlinearity is unlikely to involve n>>1 and is probably almost linear because many of the profiles are parabolic (Figure 6).

## Conclusions

The median diffusivity deduced from sediment slopes is 0.04-0.11 $m^2\ yr^{-1}$, where the range represents the uncertainty in the mean sedimentation rate used to estimate lateral fluxes. For a slope of 0.1 (6°), this corresponds to a downslope flux of 0.004-

0.011 $m^2$ per year (equivalent to a 10-cm-thick surface layer moving 10 cm downslope each year) and proportionally higher for greater slopes. The apparent diffusivity is highly variable, although the range of values may be partly due to errors in the estimation of lateral fluxes or to three-dimensional transport. If downslope transport is nonlinear, the flux is probably not dependent on a high power of slope because this would result in V-shaped deposits in basins, which are not observed.

The model diffusivity value, 0.04-0.11 $m^2$ $yr^{-1}$, suggests that the model, if verified, would be useful for studying the evolution of oceanic faults in areas of high sedimentation rates because the amount of sediment transported off the footwall would be sufficient to create unconformities and stratigraphy in surrounding basins. For example, a 6° tectonic tilt followed by $10^5$ years of sediment transport could result in up to ~400-1100 $m^2$ being removed from the footwall. (Unconformities would not be produced if $K$ were much lower because sediments would merely drape the topography.)

A simple model for differential compaction demonstrates that compaction is not the primary cause of sloping surfaces around basins because rates of surface tilting are too slow. The model assumes a linear porosity-depth function for shallow pelagic carbonates and that initially flat sediment surfaces are uniformly supplied with further sediment with no lateral transport. Using a porosity-depth regression [*Hamilton*, 1976] and assuming a sedimentation rate of 10 m m.y.$^{-1}$, the maximum rate of change of slope is typically 0.03° per m.y. per degree of basement slope and is proportionally higher for higher sedimentation rates.

As emphasized in the introduction, the approach of comparing the shapes of present-day sediment surfaces to solutions of the diffusion equation does not unequivocally prove that the diffusion equation properly represents sediment transport for those areas. Furthermore, there are some moats around basement contacts, which suggest erosion or nondeposition due to bottom currents. These are inconsistent with the diffusion model so the model is not universally applicable. However, the similarity of some surfaces to solutions to the diffusion equation suggests that further effort directed to explore this problem may be fruitful. This should, in particular, consider the mechanisms of gravity-driven transport.

## Appendix 1: Practical Application of the Diffusion Model

Further verification of the diffusion model is needed before it can be used to predict sedimentation with confidence. Application of the model is also hampered by the difficulty in predicting bottom currents, which can potentially cause higher fluxes than predicted by the diffusion model, and a method is needed to predict $K$ (this might be done by iterative comparison of predicted sedimentation rates with data from cores). However, if these uncertainties could be overcome, the model could be useful for determining how local sedimentation rates in basins are enhanced by material moved downslope from surrounding hills (and, conversely, reduced sedimentation or erosion over hill crests). The model is best applied using numerical methods [*Webb and Jordan*, 1993], but a rough calculation may be possible by computing the local curvature ($\partial^2 U/\partial x^2$) of sediment horizons in the area of interest, where surfaces are corrected for differential compaction so they represent the curvature at time of deposition. The curvature could be estimated roughly using $(Y_{i-1}+Y_{i+1}-2Y_i)/\Delta x$, where $Y_i$ is the sediment relief over a distance $\Delta x$. From (3), the enhancement of the local sedimentation rate due to gravity transport ($K\partial^2 U/\partial x^2$) could then be compared to the locally measured sedimentation rate ($\partial U/\partial t$) and to the primary input rate $S$. $S$ could be estimated from the mean separation of seismic horizons over a large area, dated from Ocean Drilling Program (ODP) cores and corrected for compaction using the porosity $\phi$ at the horizon by multiplying by $(1-\phi)/(1-\phi_0)$, where $\phi_0$ is a typical surface porosity for the type of sediment.

The following shows how the model might be applied to sedimentation over oceanic basement using DSDP/ODP core data (the data are poor so this is only an illustration of the method). Figure A1 shows an interpretation of the structure near sites 417A and 417D produced using a near-bottom hydrophone [*Purdy et al.*, 1980]. The sediments are mostly pelagic clays deposited below the carbonate compensation depth (CCD), but the lower section consists of organic claystone and chalk [*Donnelly et al.*, 1980] which may have had similar properties to the FAMOUS sediments when they were deposited. Seismic reflector 2 roughly coincides with the top of this lower section, as suggested by physical property data [*Donnelly et al.*, 1980]. Microfossil age data [*Miles and Orr*, 1980] in Figure A1 show that the sedimentation rate at site 417D has been higher in the Cretaceous (older than 65 Ma) than that at 417A, where the Cretaceous section is generally absent. The sediment supply rate $S$ can be roughly estimated from the area $A$ between seismic reflector 2 and basement from 0 to 2.3 km (1.15 X $10^5$ $m^2$) and calculating $A/l\Delta t$, where $l$ is the width of the catchment area (2300 m) and $\Delta t$ is the difference between the basement and reflector age (~23.5 m.y.). $S$ here is 2.13 m m.y.$^{-1}$ (4.11 m m.y.$^{-1}$ when corrected for compaction assuming a surface porosity of 0.72 and in situ porosity of 0.46). The sedimentation rate at the base of site 417D is 2.0±0.5 m m.y.$^{-1}$ (compaction corrected, 3.86 m m.y.$^{-1}$). From these values, the enhancement of sedimentation rate is very roughly 0.3±1.0 m m.y.$^{-1}$ at surface porosities.

Applying the diffusion equation to sedimentation on basement is not straightforward because sediment thickness must be positive everywhere, which makes the problem nonlinear [*Webb and Jordan*, 1993]. Local sedimentation rates in depressions depend on the amount of material supplied to them from the hills rather than merely the local basement curvature. However, the following may suggest how these problems might be tackled. First, the lack of a Cretaceous section at site 417A is easily predicted by (3) because the negative basement curvature suggests nondeposition. (The average sedimentation rate $S$ and (3) predict that deposition would occur if the surface curvature is greater than $-10^{-5}$ $m^{-1}$, which is almost a planar surface.) Sediment transporting downslope from the slope and hill immediately east of site 417D encounters a flat area of basement relief at site 417D. Assuming the scarp is steep, the average deposition rate at its base from the basement age to the age of reflector 2 can be computed from $2Q/\sqrt{(\pi K\Delta t)}$, which is the solution to the diffusion equation for constant flux into a uniform topography region [*Carslaw and Jaeger*, 1959, p. 75] (the assumption of a vertical scarp will result in an overestimate of the enhancement). From the size of the pelagic catchment area given by the length of profile from site 417D to the hillcrest and the average sedimentation rate, the downslope flux $Q$ is 1200-1500 $m^2$ m.y.$^{-1}$ Assuming $K$ = 0.04-0.11 $m^2$ $yr^{-1}$, the enhanced sedimentation rate at site 417D is 0.8-1.7 m m.y.$^{-1}$ at surface porosities, which is slightly higher than that estimated from the seismic stratigraphy. This could be explained if the sediment diffusivity were much higher as suggested by the lack of curvature of reflector 2. Since reflector 2 would therefore have been deposited flat, this implies that its present dip of 1.7° is due to postdepositional tilting, such as by tectonic movement on the scarp at $x$ = 2 km.

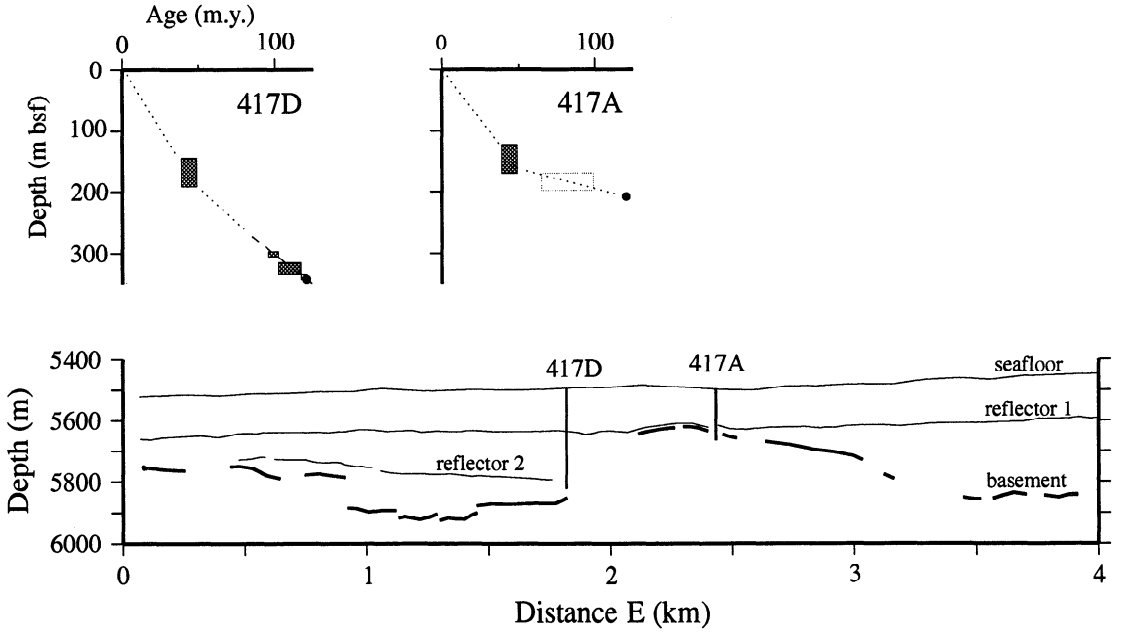


**Figure A1.** Interpreted seismic section [*Purdy et al.*, 1980] close to Deep Sea Drilling Project (DSDP) sites 417A and 417D. Depths to seismic reflectors were computed using interval travel times assuming a linear velocity-depth variation found in the physical property data for sites 417A and 417D [*Donnelly et al.*, 1980] (depth was computed from $(\exp(c_1 T/2)-1)c_0/c_1$, where $c_0$ is the surface velocity (1500 m $s^{-1}$) and $c_1$ is the velocity gradient (0.5 $s^{-1}$)). The physical property data are poor due to sediment deformation during coring but are nevertheless typical of these sediment types [*Hamilton and Bachman*, 1982]. The discrepancy between the seismically determined basement depth at site 417A (140 m) and that determined from coring (208 m) is probably due to navigational uncertainty and the basement's three-dimensional structure rather than high sediment velocities (sites 417A and 417D were 400 m and 600 m north of the section, and relative navigational uncertainty was estimated to be ~150 m [*Purdy et al.*, 1980]). The age-depth graphs shown above the section were drawn using microfossil data [*Miles and Orr*, 1980] with recent timescale revisions [*Gradstein et al.*, 1994] and with a basement age of 121 Ma (solid circles), which corresponds to the location of the drill sites in the center of magnetic anomaly M0 [*Rabinowitz et al.*, 1980]. The dashed line drawn at the base of site 417D represents a sedimentation rate of 2 m m.y.$^{-1}$. The age-depth graphs illustrate the missing Cretaceous section at site 417A but continuous section at 417D. Nondeposition at site 417A is predicted by the diffusion model from the negative basement curvature, while the enhanced sedimentation rate at 417D is lower than predicted, perhaps due to high sediment diffusivity which is suggested by the low curvature of reflector 2.

## Appendix 2: Transient Solution with Constant Fluxes

The initial condition for the problem illustrated in Figure 1a is $U(x, 0) = 0$, and the boundary conditions are $\partial U(0, t)/\partial x = -Q_1/K$ and $\partial U(W, t)/\partial x = -Q_2/K$ (sediment transporting to the right is represented by positive $Q$ as defined by (1)). Equation (4) was obtained by noting that differentiating (3) in $x$ leads to a diffusion equation for the sediment fluxes [*Carslaw and Jaeger*, 1959, p. 75]:

$$\frac{\partial Q}{\partial t} = K\frac{\partial^2 Q}{\partial x^2}. \quad \text{(A1)}$$

The solution in $Q$ for constant fluxes into a basin can therefore be taken from the similar problem of the temperature distribution of a conducting plate which has constant temperatures applied to its margins [*Carslaw and Jaeger*, 1959, p. 100]. The differential $\partial U/\partial x$ is then easily obtained using (1). The differential $\partial U/\partial t$ can be found by differentiating $\partial U/\partial x$ in $x$ and solving for $\partial U/\partial t$ using (3). The solution (equation (4)) was then found by inspection of the two partial differentials $\partial U/\partial t$ and $\partial U/\partial x$. It can be simplified slightly for studying the general form of the solution (Figure 1a) by replacing $x$ with $Wx'$ and $t$ with $W^2\tau/K$ where $x'$ and $\tau$ are dimensionless numbers. With zero $S$, the sediment topography is

$$U(x',\tau)\frac{K}{W}\frac{1}{Q_1-Q_2} = \tau - \frac{Q_1}{Q_1-Q_2}x' + \frac{x'^2}{2} + \frac{2Q_1+Q_2}{6(Q_1-Q_2)} + \frac{2}{\pi^2(Q_1-Q_2)}\sum_{n=1}^{\infty}\frac{Q_2(-1)^n-Q_1}{n^2}\cos(n\pi x')\exp(-n^2\pi^2\tau). \quad \text{(A2)}$$

## Appendix 3: Estimating Sediment Supply Rate

*Nozaki et al.* [1977] measured a rate of 29 m m.y.$^{-1}$ from radiocarbon in a core at 2500 m within the inner rift valley. Since sediment is transporting from the crestal mountains into the valley [*Marks*, 1981], this is an upper bound. *Balsam* [1988] reported a rate of 20 m m.y.$^{-1}$ (V30-88 at 2945 m); however, this was located within the transform valley of the Oceanographer fracture zone [*Fox et al.*, 1985], so it may also be an upper bound. We can perhaps infer the rate by comparison with other areas at similar latitudes. *Berger and Von Rad* [1972] found carbonate sedimentation rates of 10-30 m m.y.$^{-1}$ in Deep Sea Drilling Project cores from the eastern Atlantic off Africa and Iberia. *Berger et al.* [1994] found average rates of ~20 m m.y.$^{-1}$ for ODP Site 806, which is at 0° 19' N. *Lonsdale* [1977] used the increase in maximum thickness of sediment with distance from the East Pacific Rise at 3°S to infer a sedimentation rate of 22 m m.y.$^{-1}$. This, however, assumed that eroded or nondeposited sediments are completely removed from the area by bottom currents or are

dissolved. If instead these sediments redeposit locally in depressions, a better estimation of sedimentation rate is to regress sediment thickness on distance. Doing this for Lonsdale's data results in sedimentation rates of only 10-14 m m.y.$^{-1}$. Combining the information in these various reports, the true mean sedimentation rate in the FAMOUS area is probably between 10 and 30 m m.y.$^{-1}$ and is most likely to lie between 10 and 20 m m.y.$^{-1}$. The range 10 to 30 m m.y.$^{-1}$ was used for estimating transport rates in this study.

**Acknowledgments.** Fred Spiess and others of the Marine Physical Laboratory, Scripps Institution of Oceanography, very kindly gave me assistance and access to their database of Deep Tow records. I am grateful to Helen Webb of MIT for providing the results of her numerical modelling, which helped test the validity of using a steady state solution. I have also received advice on various aspects of sediment transport and the diffusion equation and would like to thank Bernard Coakley, Jeremy Henderson, Roger Searle, and Ken Macdonald for this. I am also grateful to T. H. van Andel for providing details of the *ALVIN* submersible observations and to Mike Leeder, James Ogg, and Helen Webb for reviewing this manuscript. Several figures were produced using the GMT software system developed by *Wessel and Smith* [1991]. Accommodation in San Diego was provided by E. A. Oakenfull of San Diego Zoo. This research was funded by a Research Fellowship from the Natural Environment Research Council. who are thanked for their support.

## References

Arrhenius, G. A., Pelagic sediments, in *The Sea*, vol. 3, *The Earth Beneath the Sea*, edited by M. N. Hill, pp. 655-727, Wiley-Interscience, New York, 1963.

Atwater, T. M., and J. D. Mudie, Block faulting on the Gorda Rise, *Science, 159,* 729-731, 1968.

Atwater, T., and J. D. Mudie, Detailed near-bottom geophysical study of the Gorda Rise, *J. Geophys. Res., 78,* 8665-8686, 1973.

Audet, D. M., Modelling of porosity evolution and mechanical compaction of calcareous sediments, *Sedimentology, 42,* 355-373, 1995.

Ballard, R. D., and J. G. Moore, *Photographic Atlas of the Mid-Atlantic Ridge Rift Valley*, 114 pp., Springer-Verlag, New York, 1977.

Balsam, W. L., Sediment accumulation rates west of the Mid-Atlantic Ridge (~35°N), *Mar. Geol., 81,* 1-13, 1988.

Begin, Z. B., D. F. Meyer, and S. A. Schumm, Development of longitudinal profiles of alluvial channels in response to base-level lowering, *Earth Surf. Processes Landforms, 6,* 49-68, 1981.

Berger, W. H., and G. R. Heath, Vertical mixing in pelagic sediments, *J. Mar. Res., 26,* 124-143, 1968.

Berger, W. H., and D. J. W. Piper, Planktonic foraminifera: Differential settling, dissolution and redeposition, *Limnol. Oceanogr., 17,* 275-287, 1972.

Berger, W. H., and U. Von Rad, Cretaceous and Cenozoic sediments from the Atlantic Ocean, *Init.ial Rep. Deep Sea Drill. Proj., 14,* 787-954, 1972.

Berger, W. H., M. K. Yasuda, T. Bickert, G. Wefer, and T. Takayama, Quaternary time scale for the Ontong Java Plateau: Milankovitch template for Ocean Drilling Program Site 806, *Geology, 22,* 463-467, 1994.

Carslaw, H. S., and J. C. Jaeger, *Conduction of Heat in Solids*, 2nd ed., 510 pp., Oxford Univ. Press, New York, 1959.

Carson, M. A., and M. J. Kirkby, *Hillslope Form and Process*, 475 pp., Cambridge Univ. Press, New York, 1972.

Culling, W. E. H., Analytical theory of erosion, *J. Geol., 68,* 336-344, 1960.

Culling, W. E. H., Theory of erosion on soil-covered slopes, *J. Geol., 73,* 230-254, 1965.

Donnelly, T., et al., *Initial Reports of the Deep Sea Drilling Project*, vol. 51, 52, and 53, 718 pp., U.S. Govt. Print. Off., Washington, D.C., 1980.

Flemings, P. B., and T. E. Jordan, A synthetic stratigraphic model of foreland basin development, *J. Geophys. Res., 94,* 3851-3866, 1989.

Forbes, D. L., and G. Drapeau, Near-bottom currents and sediment transport on the inner Scotian Shelf: Sea-floor response to winter storms during CASP, *Atmos. Ocean, 27,* 258-278, 1989.

Fox, P, J., et al., The geology of the Oceanographer Transform: The transform domain, *Mar. Geophys. Res., 7,* 329-358, 1985.

Gradstein, F. M., F. P. Agterberg, J. G. Ogg, J. Hardenbol, P. van Veen, J. Thierry, and Z. Huang, A Mesozoic time scale, *J. Geophys. Res., 99,* 24,051-24,074, 1994.

Gross, T. F., and A. R. M. Nowell, Turbulent suspension of sediments in the deep sea, *Philos. Trans. R. Soc. London A, 331,* 167-181, 1990.

Gross, T. F., A. J. Williams, and A. R. M. Nowell, A deep-sea sediment transport storm, *Nature, 331,* 518-521, 1988.

Hamilton, E. L., Variations of density and porosity with depth in deep-sea sediments, *J. Sediment. Petrol., 46,* 280-300, 1976.

Hamilton, E. L., and R. T. Bachman, Sound velocity and related properties of marine sediments, *J. Acoust. Soc. Am., 72,* 1891-1904, 1982.

Karato, S., and K. Becker, Physical properties of sediments from the Galapagos region and their implications for hydrothermal convection, edited by J. Honnorez et al., *Initial Rep. Deep Sea Drill. Proj., 70,* 355-368, 1983.

Kastens, K. A., K. C. Macdonald, S. P. Miller, and P. J. Fox, Deep Tow studies of the Vema Fracture Zone, 2, Evidence for tectonism and bottom currents in the sediments of the transform valley floor, *J. Geophys. Res., 91,* 3355-3367, 1986.

Keller, G. H., S. H. Anderson, and J. W. Lavelle, Near-bottom currents in the Mid-Atlantic Ridge rift valley, *Can. J. Earth Sci., 12,* 703-710, 1975.

Kenyon, P. M., and D. L. Turcotte, Morphology of a delta prograding by bulk sediment transport, *Bull. Geol. Soc. Am., 96,* 1457-1465, 1985.

Kirkby, M. J., *Hillslope process - response models based on the continuity equation*, *Spec. Publ., Trans. Inst. Brit. Geogr., 3,* 1971.

Klitgord, K. D., and J. D. Mudie, The Galapagos spreading centre: A near-bottom geophysical survey, *Geophys. J. R. Astron. Soc., 38,* 563-586, 1974.

Langseth, M. G., K. Becker, R. P. Von Herzen, and P. Schultheiss, Heat and fluid flux through sediment on the western flank of the Mid-Atlantic Ridge: A hydrogeological study of North Pond, *Geophys. Res. Letts, 19,* 517-520, 1992.

Lonsdale, P., Structural geomorphology of a fast-spreading rise crest: The East Pacific Rise near 3° 25'S, *Mar. Geophys. Res., 3,* 251-293, 1977.

Luyendyk, B. P., Origin and history of abyssal hills in the Northeast Pacific Ocean, *Geol. Soc. Am. Bull., 81,* 2237-2260, 1970.

Luyendyk, B. F., and K. C. Macdonald, Physiography and structure of the inner floor of the FAMOUS rift valley: Observations with a deep-towed instrument package, *Bull. Geol. Soc. Am., 88,* 648-663, 1977.

Macdonald, K. C., and B. P. Luyendyk, Deep-tow studies of the structure of the Mid-Atlantic Ridge crest near latitude 37° N, *Geol. Soc. Am. Bull., 88,* 621-636, 1977.

Marks, N. S., Sedimentation on new ocean crust: The Mid-Atlantic Ridge at 37°N, *Mar. Geol., 43,* 65-82, 1981.

Miles, G. A., and W. N. Orr, Planktonic foraminifers from the Bermuda Rise, Deep Sea Drilling Project Legs 51, 52 and 53, edited by T. Donnelly et al., *Initial Rep. Deep Sea Drill. Proj., 51, 52, 53,* Part 2, 791-813, 1980.

Mitchell, J. K., *Fundamentals of Soil Behavior*, 422 pp., John Wiley, New York, 1976.

Mitchell, N. C., A model for attenuation of backscatter due to sediment accumulations and its application to determine sediment thickness with GLORIA sidescan sonar, *J. Geophys. Res., 98,* 22,477-22,493, 1993.

Mitchell, N. C., Characterising the extent of volcanism at the Galapagos Spreading Centre using Deep Tow profiler records, *Earth Planet. Sci. Lett.,* in press, 1995.

Nozaki, Y., J. K. Cochran, K. K. Turekian, and G. Keller, Radiocarbon and $^{210}$Pb distribution in submersible-takend deep-sea cores from project FAMOUS, *Earth. Planet. Sci. Lett., 34,* 167-173, 1977.

Prior, D. B., and J. N. Suhayda, Application of infinite slope analysis to subaqueous sediment instability, Mississippi Delta, *Eng. Geol., Amsterdam, 14,* 1-10, 1979.

Purdy, G. M., J. I. Ewing, and G. M. Bryan, A deep-towed hydrophone seismic-reflection survey around IPOD sites 417 and 418, *Mar. Geol., 35,* 1-19, 1980.

Rabinowitz, P. D., H. Hoskins, and S. M. Asquith, Geophysical site survey results near Deep Sea Drilling Project sites 417 and 418 in the central Atlantic Ocean, edited by T. Donnelly et al., *Initial Rep. Deep Sea Drill. Proj., 51, 52, 53,* 629-669, 1980.

Ruddiman, W. F., Sediment redistribution on the Reykjanes Ridge: Seismic evidence, *Geol. Soc. Am. Bull., 83,* 2039-2062, 1972.

Seibold, E., and D. Futterer, Sediment dynamics on the Northwest African continental margin, in *The Ocean Floor*, edited by R. A. Scrutton and M. Talwani, pp. 147-163, John Wiley, New York, 1982.

Shaw, P. R., and J. Lin, Causes and consequences of variations in faulting

style at a Mid-Atlantic Ridge, *J. Geophys. Res., 98,* 21,839-21,851, 1993.

Shor, A., P. Lonsdale, C. D. Hollister, and D. Spencer, Charlie-Gibbs fracture zone: bottom-water transport and its geological effects, *Deep Sea Res., Part A, 27,* 325-345, 1980.

Sinclair, H. D., B. J. Coakley, P. A. Allen, and A. B. Watts, Simulation of foreland basin stratigraphy using a diffusion model of mountain belt uplift and erosion: An example from the central Alps, Switzerland, *Tectonics, 10,* 599-620, 1991.

Spiess, F. N., and P. F. Lonsdale, Deep Tow rise crest exploration techniques, *Mar. Technol. Soc. J., 16,* 67-74, 1982.

Spiess, F. N., and R. C. Tyce, Marine Physical Laboratory Deep Tow instrumentation system, *SIO Ref. 73-4,* Mar. Phys. Lab. of the Scripps Inst. of Oceanogr., Univ. of Calif., San Diego, 1973.

Van Andel, T. H., and P. D. Komar, Ponded sediments of the Mid-Atlantic Ridge between 22° and 23° North latitude, *Geol. Soc. Am. Bull., 80,* 1163-1190, 1969.

Vogt, P. R., and G. L. Johnson, A longitudinal seismic reflection profile of the Reykjanes Ridge, I, Evidence for west-flowing bottom water, *Earth Planet. Sci. Lett., 18,* 45-48, 1973.

Webb, H. F., and T. H. Jordan, Quantifying the distribution and transport of pelagic sediments on young abyssal hills, *Geophys. Res. Lett., 20,* 2203-2206, 1993.

Wessel, P., and W. H. F. Smith, Free software helps map and display data, *Eos Trans. AGU, 72,* 441, 445-446, 1991.

Whitmarsh, R. B., and A. S. Laughton, A long range sonar study of the Mid-Atlantic Ridge crest near 37°N (FAMOUS area) and its tectonic implications, *Deep Sea Res., 23,* 1005-1023, 1976.

N. C. Mitchell, Department of Geological Sciences, University of Durham, Science Laboratories, South Road, Durham DH1 3LE, England. (e-mail: n.c.mitchell@durham.ac.uk)

(Received December 28, 1994; revised June 13, 1995; accepted June 21, 1995.)